THERMAL MODELING OF WORKPIECE TEMPERATURE AND DISTORTION IN MQL DEEP-HOLE DRILLING

by

Li-Jung Tai

A dissertation submitted in partial fulfillment
of the requirements for the degree of
Doctor of Philosophy
(Mechanical Engineering)
in The University of Michigan
2011

Doctoral Committee:

Professor Albert J. Shih, Chair
Professor John E. Allison
Professor Jun Ni
Richard J. Furness, Ford Motor Company
David A. Stephenson, Ford Motor Company

ACKNOWLEDGEMENTS

I truly appreciate the support that I have received from all directions.

First, my deepest gratitude is to my advisor, Professor Albert Shih, for always sharing with me his vast knowledge and providing me stimulating suggestions. I am deeply grateful to him for the long discussions that helped me sort out the technical details of my work and improve the quality of my paper. His enthusiasm in research has truly inspired me along the way. I greatly appreciate his great help and sincere advice on my future career development.

I would like to thank my committee member, Professor Jun Ni, the director of Wu Manufacturing Research Center (WuMRC), where I have conducted my research in the past years. This research topic is deeply inspired by Professor Sam Wu's (the founder of WuMRC) dedication to the manufacturing world and the tradition of this research center on machining process development. The basis of this research is also on one of Professor Ni's research achievements. I am grateful to have his inputs in this research.

I am also extremely grateful to Dr. Richard Furness for providing me the opportunity to conduct experiments in the advance manufacturing technology development (AMTD) lab at Ford motor company. The research aims to produce practical value through analyzing the data from production system. This goal will never be achieved without his support and the AMTD lab. I would also like to thank him for being my committee member and providing valuable suggestions from the viewpoints of academic and industrial needs.

Very special thanks go to Dr. David Stephenson, who was my co-advisor while being a research scientist here. I value the time he has spent with me and I am grateful to have worked with him closely these past few years. He guided me through the machining science with his broad knowledge in this area. I greatly enjoyed and benefited through his advice.

I would like to extend my gratitude to my other committee member, Professor John Allison for his constructive suggestions and valuable discussion along my studies.

I would like to thank all of my colleagues at the WuMRC Lab for providing a great environment to learn and do research. I thank Steve Erskine, our lab supervisor, for instructing me in CNC machines. I thank Andrew Jessop for his assistance in the experiments. I thank Steve White for his guidance on writing papers. I am also grateful to my friends outside the lab who have enriched my PhD life.

Most importantly, I would like to thank my Mom, Dad, and brother, Kirk, for their unwavering support and encouragement. While there have been several difficult moments in the beginning of my PhD study, they provided the love and strength that have made me who I am today.

TABLE OF CONTENTS

LIST OF FIGURES

LIST OF TABLES

CHAPTER 1
INTRODUCTION

1.1 Motivation

Minimum quantity lubrication (MQL) machining processes have been widely implemented in automotive powertrain production and demonstrated the benefits to reduce the manufacturing cost and environmental impact. In conventional flood cooling, the usage of a large amount of cutting fluid can potentially cause ground contamination, evaporation and dissociation of emulsion, energy consumption, wet chip disposal and some other healthy and safety issues. Maintaining and operating such fluid supplies is a high cost driver and an environmental challenge. In addition, the flood cooling system also takes the floor space and limits the flexibility to relocate machines in the production line [1].

MQL is achieved by using a small amount of oil-based lubricant mixed with pressurized air to generate droplet and deliver directly to the tool cutting edge. The lubricant flow rate in MQL application is typically 10-100 mL/h, which is a reduction in fluid flow of over 20,000 times compared with conventional flood machining [2]. Another benefit of this method is that both parts and chips remain nearly dry when MQL is properly applied, which reduces the cost of processing chips for recycle [3]. Automotive industry has implemented the MQL machining in production. Ford Motor Company is the leader of applying MQL to aluminum prismatic parts production and has 100% MQL application in transmission housing manufacturing and other powertrain component production. However, in some machining operations, such as the drilling of the cross and oil holes in steel crankshaft, MQL has not been widely implemented due to

the limited tool life and workpiece thermal distortion [4]. This research is aimed to study the MQL for deep hole drilling.

MQL has also been studied in many machining processes such as drilling [5,6], milling [7-10], turning [11-14] and grinding [15-19]. The results of these studies showed that with a proper selection of the MQL system and cutting parameters, it is possible for MQL machining to obtain performances similar to flood lubricated conditions, in terms of lubricity, tool life, and surface finish.

To completely substitute conventional flood cooling, MQL has to deliver three primary functions: lubrication, cooling and chip evacuation. However, since a small amount of fluid is applied, the heat dissipation in MQL machining is not as efficient as flood cooling. The high temperature around the cutting region may cause workpiece thermal distortion and poor dimensional accuracy. Particularly for the high energy density machining processes, such as the deep-hole drilling, the extreme thermal load makes it difficult to achieve stringent dimensional tolerances of precision automotive powertrain parts.

Deep-hole drilling with length to diameter ratio larger than 10 is a high-energy-density machining process which requires good lubrication and cooling to maintain tool life and hole quality. MQL in deep-hole drilling application is a relatively new area with little previous research. Heinemann et al. [6] presented that with the external MQL supply, the tool life decreased with the increasing hole depth, whereas low-viscous type lubricant with high-cooling capacity could help maintain the tool life. Filipovic and Stephenson [4] reported that MQL drilling can yield tool life equivalent to gun drills at higher penetration rates in steel and nodular iron, while the thermal expansion in machining aluminum could be a challenge due to its low heat capacity and high expansion coefficient. Hussain et al. [20] demonstrated that the MQL deep-hole drilling is feasible in production with optimal feed and speed. The workpiece surface temperature could vary significantly under different feeds and speeds.

High temperature in deep-hole drilling can lead to many detrimental effects, such as workpiece dimensional errors and shorter tool life from high thermal stress. Since the heat generation rate and drill temperature distribution are difficult to measure directly, numerical modeling becomes an important tool to study the drilling temperature. Agapiou

and Stephenson [21] have reviewed the early analytical modeling of temperature distribution in the drill, which is mostly represented as a semi-infinite body. The empirical force equations from a series of oblique cutting tests were used to calculate heat source, and a transient heat transfer analysis was carried out to calculate the heat partition [22, 23]. On the analysis of the drill as a finite domain, Saxena et al. [24] and Watanabe et al. [25] have applied the finite difference method. In more recent work, finite element analysis (FEA) has been applied by Fuh [26], Chen [27], and Bono and Ni [28-30] for the drill temperature analysis. Li and Shih [31,32] utilized the finite element analysis with heat inverse model to more accurately predict the drill temperature.

Most of proposed studies were focused on the temperature distribution on the drill to evaluate the tool wear, but limited research is on the prediction of temperature distribution in the workpiece. The thermal expansion on the workpiece can lead to errors in the size and location of drilled holes. The hole geometry often presents a taper shape after dry drilling with a smaller diameter at the entry due to the thermal expansion on the drill and workpiece [29,33]. The research on hole position errors due to workpiece thermal distortion is still lacking. In MQL deep-hole drilling, a large amount of heat can be conducted from the chips in the hole during evacuation. The thermally induced workpiece distortion can cause the hole position error or machining error for the follow-up operations. The hole shape may be also affected by the clamping layout on the workpiece. Therefore, a more comprehensive thermal model of the workpiece in MQL deep-hole drilling is needed to investigate the heat generation and thermal distortion effects.

1.2 Research objectives

The focus of this research is on determination of heat flow into the workpiece during MQL deep-hole drilling. There is a lack of understanding on the significance of HWS heat flux and how it is related to different machining conditions. Therefore, a thermal modeling method is developed to quantify the heat fluxes in this study. This model will be utilized to investigate the workpiece temperature under different machining conditions and to develop a thermal-elastic model to predict the workpiece thermal distortion. The specific tasks include:

(1) To develop an inverse heat transfer method for deep-hole drilling to quantify the HBS heat flux and the spatial and temporal distribution of HWS heat flux. The HBS heat flux is compared with the theoretical calculation. The HWS heat flux is validated by the measured temperature.

(2) To apply the inverse heat transfer method to investigate the effects of air pressure and drilling feed rate on workpiece temperature in MQL deep-hole drilling. The change of HWS heat flux and the significance in the workpiece temperature under different conditions are compared.

(3) To develop a 3-D thermal-elastic coupled FEA to predict the workpiece temperature and associated distortion in drilling multiple deep-holes under MQL condition. The model aims to be practical and accurate without extensive computation.

Fulfillment of the objectives will provide a comprehensive understanding of the heat flow into workpiece in MQL deep-hole drilling and the effects of different machining conditions on the workpiece temperature. The 3-D FEA will provide an accurate and efficient prediction of the workpiece thermal distortion, thus it can be involved in practical applications, such as error compensation and design of the clamping layout.

1.3 Organization of the dissertation

This dissertation is presented in a multiple manuscript format. Chapters 2, 3, and 4 are written as individual research papers, including the abstract, the main body and the references.

Chapter 2 presents a workpiece thermal model for drilling and an inverse heat transfer method to calculate the HBS and HWS heat fluxes. Experimental studies in both dry and MQL deep-hole drillings are conducted to validate this method.

Chapter 3 investigates the effects of air pressure and feed rate on workpiece temperature in MQL deep-hole drilling. Experiments are conducted with the production dual-channel through spindle MQL system and analyzed by the inverse heat transfer method.

Chapter 4 proposes a 3-D FEA model to predict the thermal distortion of workpiece caused by drilling multiple deep-holes. The validation is conducted through experimentally measured workpiece temperature and expansion.

Chapter 5 draws the conclusions and summarizes the original contributions of the dissertation. Several topics are also proposed for future research.

References

[1] Stoll, A., Sebastian, A.J., Klosinski, R., and Furness R., 2008, “minimum quantity lubrication (MQL) is a key technology for driving the paradigm shift in machining operations,” SAE Paper 01-1128.

[2] Autret, R. and Liang, S.Y., 2003, “Minimum quantity lubrication in finish hard turning,” HNICEM ’03.

[3] Itoigawa, F., Childs, T.H.C., Nakamura, T., and Belluco, W., 2006, “Effects and mechanisms in minimal quantity lubrication machining of an aluminum alloy," Wear, 260, pp. 339-344.

[4] Filipovic, A. and Stephenson, D., 2006, “Minimum quantity lubrication (MQL) application in automotive powertrain machining,” Machining Science & Technology, 10, pp. 3-22.

[5] Braga, D.U., Diniz, A.E., Miranda, G.W.A., and Coppini, N.L., 2002, “Using a minimum quantity of lubricant (MQL) and a diamond coated tool in the drilling of aluminum-silicon alloys,” Journal of Materials Processing Technology, 122, pp. 127-138.

[6] Heinemann, R., Hinduja, S., Barrow, G., and Petuelli, G., 2006, “Effect of MQL on the tool life of small twist drills in deep-hole drilling,” International Journal of Machine Tools and manufacture, 46, pp. 1-6.

[7] Rahman, M., Senthil Kumar, A., and Salam, M. U., 2001, “Evaluation of minimal quantities of lubricant in end milling,” International Journal of Advanced Manufacturing Technology, 18, pp. 235-241.

[8] Lopez de Lacalle, L.N., Angulo, C., Lamikiz, A., and Sanchez, J.A., 2006, “Experimental and numerical investigation of the effect of spray cutting fluids in high speed milling,” Journal of Materials Processing Technology, 172, pp. 11-15.

[9] Su, Y.L., Liu, T.H., Su, C.T., Yao, S.H., Kao, W.H., and Cheng, K.W., 2006, “Wear of CrC-coated carbide tools in dry machining,” Journal of Materials Processing Technology, 171, 108-117.

[10] Liao, Y.S. and Lin, H.M., 2007, “Mechanism of minimum quantity lubrication in highspeed milling of hardened steel,” International Journal of Machine Tools and Manufacture, 47, pp. 1660-1666.

[11] Wakabayashi, T., Sato, H., and Inasaki, I., 1998, “Turning using extremely small amounts of cutting fluids,” JSME International Journal, 41, pp. 143-148.

[12] Dhar, N.R., Islam, M.W., Islam, S., and Mithu, M.A.H., 2006, “The influence of minimum quantity of lubrication (MQL) on cutting temperature, chip and dimensional accuracy in turning AISI-1040 steel,” Journal of Materials Processing Technology, 171, pp. 93-99.

[13] Davim, J.P., Sreejith, P.S., and Silva, J., 2007, “Turning of brasses using minimum quantity of lubricant and flooded lubricant conditions,” Materials and Manufacturing Processes, 22, pp. 45-50.

[14] Kamata, Y. and Obikawa, T., 2007, “High speed MQL finish-turning of Inconel 718 with different coated tools,” Journal of Materials Processing Technology, 192, pp. 281-286.

[15] Baheti, U., Guo, C., and Malkin, S., 1998, “Environmentally conscious cooling and lubrication for grinding,” Proceedings of the International Seminar on Improving Machine Tool Performance, 2, pp. 643-654.

[16] Hafenbraedl, D., and Malkin, S., 2000, “Environmentally-conscious minimum quantity lubrication (MQL) for internal cylindrical grinding,” Transactions of NAMRI/SME, 28, pp. 149-154

[17] Silva, L.R., Bianchi, E.C., Catai, R.E., Fusse, R.Y., and Franca, T.V., 2005, “Study on the behavior of the minimum quantity lubricant - MQL technique under different lubricating and cooling conditions when grinding ABNT 4340 steel,” Journal of the Brazilian Society of Mechanical Sciences and Engineering, 27, pp. 192-199.

[18] Shen, B., Shih, A.J., and Tung, S.C., 2008, “Application of nanolfuids in minimum quantity lubrication grinding,” Tribological Transactions, 51, pp. 730-737.

[19] Shen, B., Malshe, A.P., Klita, P., and Shih, A.J., 2008, “Performance of novel MoS_2 nanoparticles based grinding fluids in minimum quantity lubrication grinding,” Transactions of NAMRI/SME, 36, pp. 357-364.

[20] Hussain, M.I., Taraman, K.S., Filipovic, A.J., and Garren, I., 2008, "Experimental study to analyse the workpiece surface temperature in deep hole drilling of aluminum alloy engine blocks using MQL technology," Journal of Achievement in Materials and Manufacturing Engineering, 31, pp. 485-490.

[21] Stephenson, D.A. and Agapiou, J.S., 2006, Metal Cutting Theory and Practice, 2nd Edition, Taylor and Francis, Boca Raton, FL.

[22] Agapiou, J.S. and DeVries, M.F., 1990, "On the determination of thermal phenomena during drilling- part I and II," International Journal of Machine Tools and Manufacture, 30, pp. 203-226.

[23] Agapiou, J.S. and Stephenson, D.A., 1994, "Analytical and experimental studies of drill temperature," Transactions of the ASME, 116, pp.54-60.

[24] Saxena, U.K., DeVries, M.F., and Wu, S. M., 1971, "Drill temperature distributions by numerical solutions," Journal of Engineering for Industry, 93, pp. 1057-1065.

[25] Watanabe, K., Yokoyama, K., and Ichimiya, R., 1977, "Thermal Analyses of the Drilling Process," Bulletin of the Japan Society of Precision Engineering, 11, pp. 71-77.

[26] Fuh, K. H., 1987, "Computer aided design and manufacturing of multi-facet drills," PhD Dissertation, University of Wisconsin at Madison.

[27] Chen, W.C., 1996, "Effect of the cross-sectional shape design of a drill body on drill temperature distributions," International Communications in Heat and Mass Transfer, 23, pp. 355-366.

[28] Bono, M. and Ni, Jun, 2001, "The effects of thermal distortions on the diameter and cylindricity of dry drilled holes," International Journal of Machine Tools & Manufacture, 41, pp.2261-2270

[29] Bono, M. and Ni, Jun, 2002, "A model for predicting the heat flow into the workpiece in dry drilling," Journal of Manufacturing Science and Engineering, 124, pp. 773-777.

[30] Bono, M. and Ni, J., 2006, "The location of the maximum temperature on the cutting edges of a drill, " International Journal of Machine Tools & Manufacture, 46, pp.901-907.

[31] Li, R. and Shih, A.J., 2007, "Tool temperature in titanium drilling," Journal of Manufacturing Science and Engineering, 129, pp. 740-749.

[32] Li, R. and Shih, A.J. 2007, "Finite element modeling of high-throughput drilling of Ti-6Al-4V," Transactions of NAMRI/SME, pp. 73-80.

[33] Kalidas, S., Kapoor, S.G., and DeVor, R.E., 2002, "Influence of thermal effects on

hole quality in dry drilling, part 2: thermo-elastic effects on hole quality,” Journal of Manufacturing Science and Engineering, 124, pp.267-274

CHAPTER 2

AN INVERSE HEAT TRANSFER METHOD FOR DETERMINING WORKPIECE TEMPERATURE IN MQL DEEP HOLE DRILLING

ABSTRACT

This study investigates the workpiece temperature in minimum quantity lubrication (MQL) deep hole drilling. An inverse heat transfer method is developed to estimate the spatial and temporal change of heat flux on the drilled hole wall surfaces based on the workpiece temperature measured using embedded thermocouples and analyzed using the finite element method. The inverse method is validated experimentally in both dry and MQL deep-hole drilling conditions, and the results show good agreement with experimental temperature measurements. This study demonstrates that the heat generated on the hole wall surface is significant in deep hole drilling. In the example studied on deep hole drilling of iron, the level of heat applied on the hole wall surface is about the same as the heat applied on the hole bottom surface when a 10 mm drill reached a depth of 120 mm.

Contents of this chapter have been submitted as Tai, B.L., Stephenson, D.A., and Shih, A.J., (2011), "An Inverse Heat Transfer Method for Determining Workpiece Temperature in MQL Deep Hole Drilling," *Journal of Manufacturing Science and Engineering*

Nomenclature

h_b: Heat flux on the drilled hole bottom surface (HBS)

h_w: Heat flux on the drilled hole wall surface (HWS)

h_w^{pq}: Heat flux applied on Segment #p of HWS at time step q

P: Total number of segments

T^i: Temperature at Input Point #i

T_b^i: Temperature at Input Point #i generated by h_b

T_w^i: Temperature at Input Point #i generated by h_w

$T_{w\_exp}^{\ i}$:Temperature at Input Point #i calculated by subtracting $T_b^{\ i}$ from measured T^i

I^{ijpq}: Impact tensor

T_u: Temperature at Input Point #1 generated by h_b = 1.0 MW/m^2

k: Scale factor for adjusting the magnitude of T_u

a: Length between input points and the segment size along HWS

w: Diameter of the cylindrical workpiece

l: Length of the cylindrical workpiece

D: Diameter of the drill

x_1, x_2, x_3, x_4 : Axial positions of control points from the drill cutting edge

c_0: Initial heat flux value of control points

c_{11}, c_{21}, c_{31}, c_{12}, c_{22}, c_{32}: Coefficients of time-dependent heat flux values of control points

2.1 Introduction

Minimum quantity lubrication (MQL) utilizes a minute amount of metal working fluid via droplet form during the machining process. MQL is being increasingly used in automotive powertrain manufacturing, not only for the environmental benefits but also for cost and quality improvements over traditional flood cooling [1,2]. One of the technical barriers to full implementation of MQL in machining operations for powertrain components is the deep hole drilling. The high workpiece temperature and associated hole thermal distortion in MQL deep hole drilling presents practical problems. Deep hole drilling refers to a drilling process with a length to diameter ratio over 10. It is a high energy density process commonly used in drilling operations of crankshaft oil holes, transmission valve body spool bores, and engine block oil feed holes. Although MQL has achieved performance equal or better than flood cooling in many machining operations [3-6], MQL for deep hole drilling has not been widely implemented in the high-volume production. One of the technical challenges is the high workpiece temperature that results in hole thermal distortion. A comprehensive understanding of the workpiece heat transfer in deep hole drilling can help in the selection of better MQL and machining parameters and reduce the hole dimensional errors.

The thermal analysis of drilling has mostly concentrated on investigating the drill temperature. Stephenson and Agapiou [7,8] reviewed the analytical modeling of drill temperatures. Recent applications of finite element analysis (FEA) to study drill temperature were reviewed by Bono and Ni [9] and Li and Shih [10]. For analyzing the workpiece temperature in drilling, Bono and Ni [11,12] proposed an advection model to predict the workpiece temperature and hole distortion in dry drilling. This model assumes the heat flux only occurred on the hole bottom surface (HBS), as marked in Fig. 2.1, and is suitable for drilling shallow holes. For deep hole drilling, heat sources on the hole wall surface (HWS marked in Fig. 2.2) could be significant due to the friction between drill margins and workpiece, chip accumulated in the drill for evacuation [13], and heat transfer from high temperature drill to the workpiece. This study addresses the need of developing a deep hole drilling workpiece thermal model by considering the heat generation on both HBS and HWS.

The inverse heat transfer method is applied to find the heat flux on HBS and HWS. This method has been adopted and developed by Li and Shih [14] for drill temperature analysis. The heat flux at the drill cutting edge was calculated based on measured temperatures using embedded thermocouples in the drill. In this study, thermocouples are embedded in the workpiece near the drilled hole surface. The measured workpiece temperature at some thermocouple locations is the input for inverse heat transfer model to calculate the heat flux on HBS and HWS. The HBS and HWS heat flux are utilized to analyze workpiece temperature, which is validated at other thermocouple locations embedded in the workpiece.

In this paper, the concept of the inverse heat transfer method for determining heat flux applied on workpiece in drilling is first introduced in Sec. 2.2 The experimental setup for validation of the inverse method is presented in Sec. 2.3. This is followed by analysis and calculation of heat fluxes in Secs. 2.4 and 2.5. The temperature distribution of workpiece calculated from obtained heat fluxes will be presented and discussed in Sec. 2.6.

2.2 Inverse heat transfer method

Two heat fluxes on the workpiece to be solved for are denoted as h_b on HBS and h_w on HWS in deep hole drilling. Temperature data obtained by embedded thermocouples along the depth and close to the hole surface are used as the input to solve these two unknown heat fluxes. These thermocouple locations are defined as input points. Optimization is used to find the corresponding h_b and h_w by minimizing an objective function consisting of the discrepancy of measured and FEA temperature at input points.

The temperature rise in the workpiece at Input Point #*i* (thermocouple #*i*) is assumed to be the superposition of the temperatures T_b^i and T_w^i from heat fluxes h_b and h_w, respectively.

$$T^i(t) = T_b^i(t) + T_w^i(t) \tag{2.1}$$

The inverse method is conducted by the following steps to estimate h_b and h_w. First, h_b, which is mainly from the drill tip cutting edge induced heat, is calculated based on the measured temperature at the thermocouple closest to the hole entry surface. The procedure to calculate h_b is outlined in Sec. 2.2.2. The workpiece temperature at each input point obtained by applying only h_b is denoted as T_b^i. Then, $T_{w\_exp}^i$ is calculated by subtracting T_b^i from the measured temperature T^i. $T_{w\_exp}^i$ is used to find the heat flux h_w. Two approaches are proposed in Secs. 2.2.3 and 2.2.4 to determine h_w.

2.2.1 Finite element model for workpiece thermal analysis

FEA of the workpiece temperature was performed using ABAQUS. Figure 2.1 shows the two-dimensional axisymmetric mesh. Diameters of the workpeice and drill are denoted as w and D, respectively. The length of workpiece is l. Four-node linear axisymmetric quadratic element (DCAX4) was selected in this study. As the drill penetrates into the workpiece, layers of five elements are sequentially removed and heat flux h_b is applied to each subsequent layer of elements. This is the advection process [12], which mimics the material removal and the moving heat source applied to the HBS in drilling. The effect of chip evacuation, which is not considered in advection process, will be included in the estimation of heat flux on the HWS.

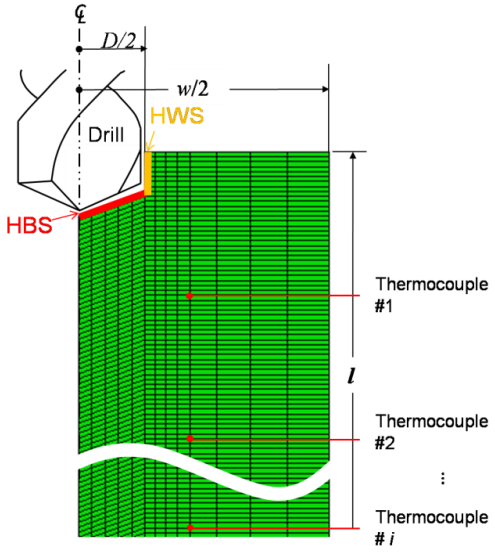

Figure 2.1 Hole wall surface (HWS), hole bottom surface (HBS) and the 2-D axisymmetric finite element mesh

In this study, the workpiece was 150 mm long (l) and 40 mm in diameter (w), while the drill was 10 mm in diameter (D). Advection models of 200, 400 and 800-layer mesh along the hole depth were evaluated. The model of 400-layer mesh was adequate since the difference in temperature between the 400- and 800-layer mesh was less than 2%. Natural convection of 10 W/m^{2}K was applied on the boundaries of the workpiece.

2.2.2 Determination of heat flux h_b on HBS

When the drill is passing a measurement point, the h_b is reflected on the temperature response first since it is ahead of h_w in the drilling direction. This is illustrated schematically in Fig. 2.2 where T^i is dominated by T_b^i initially. This phenomenon is used to find h_b using the rising (before peak) portion of measured temperature T^i at the thermocouple located closest to the hole entry (i = 1 or thermocouple #1). In the area near the top surface of workpiece, the heat flux from HWS is not significant and $T^i \approx T_b^i$

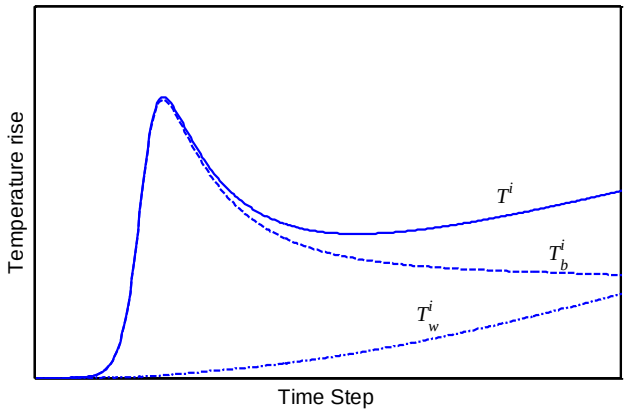

Figure 2.2 Workpiece temperature T^i by the superposition of T_b^i and T_w^i

The heat flux h_b is assumed to be time-independent through the drilling process and uniformly applied on HBS. The time-independent heat flux on the drill cutting edge was adopted in [11,12], in which the thrust force and torque on the cutting edge were assumed constant through the drilling process. Under these two assumptions, the

temperature at Input Point #1 is proportional to the temperature profile generated by an unit h_b (=1 MW/m^2), denoted as $T_u(t)$ in Fig. 2.3. A scale factor k is used to fit the measured temperature at Input Point #1 prior to the peak temperature using the following objective function.

$$\begin{aligned} &\min \sum_{t=1}^{t} \left| kT_u(t) - T^i(t) \right|, i = 1 \\ &\text{subject to} \quad k \geq 0 \end{aligned} \tag{2.2}$$

The solution of k is the h_b in the unit of MW/m^2. The result of h_b can be used to calculate $T_b^i(t)$ in the workpiece using FEA.

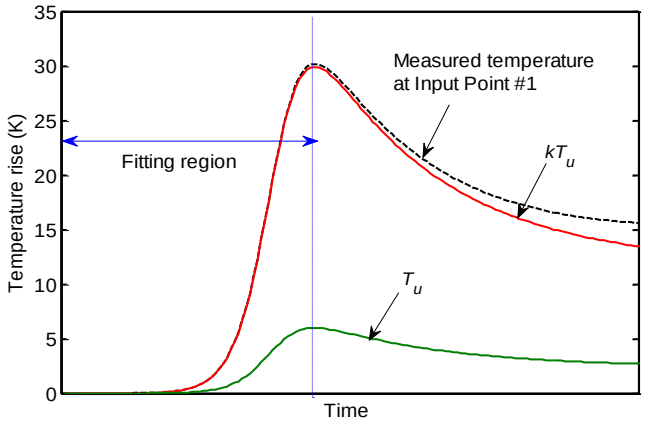

Figure 2.3 The fitting process of h_b using temperature response to different factor k.

2.2.3 Determination of h_w - Approach #1

In contrast to h_b, the heat flux h_w on HWS varies with time and drilling depth as the margin engagement and frictional heating increase. Two approaches are proposed to determine h_w. Approach #1 divides the drilled hole into P segments, as shown in Fig. 2.4, and each segment has its own heat flux and input point. In each segment, h_w is assumed to be uniformly distributed and varying with time.

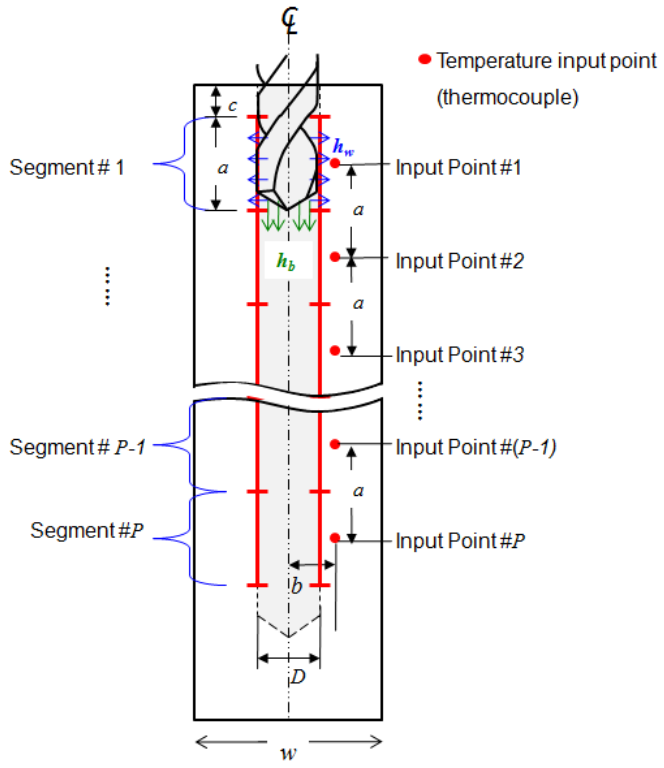

Figure 2.4 Segments and temperature input points (thermocouple locations) along the hole depth in the model

Since the temperature T_w at one point is the accumulated result of heat fluxes from different segments at different times, the relationship between the heat flux on P segments and the temperature at Input Point #i can be described in tensor as:

$$T_w^{ij} = I^{ijpq} h_w^{pq} \tag{2.3}$$

where $T_w{}^{ij}$ is the temperature response at Input Point #i and time step j, I^{ijpq} is a fourth-order impact tensor, and $h_w{}^{pq}$ is the heat flux h_w on Segment #p at time step q. Note that q and j both refer to the same drilling time with q representing the time step for the heat flux segments on HWS and j representing the time step for temperature input points.

The tensor I^{ijpq} is obtained using FEA by calculating the temperature response to a unit heat flux at a single time step. The matrix tensor $h_w{}^{pq}$ can be solved by optimization with the objective function

$$\min \sum_{i=1}^{p} \sum_{j=1}^{q} \left| T_w^{ij} - T_{w\_\exp}^{ij} \right| \tag{2.4}$$

where T_w^{ij} is calculated by Eq. (2.3) using h_w^{pq} generated from optimization iteration, and $T_{w\_exp}^{ij}$ is obtained by subtracting calculated T_b^i from experimentally measured T^i at each time step j. The sequential quadratic programming (SQP) [15] method was adopted to solve the optimization problem. Since h_w^{pq} is the unknown in this method, the given $T_{w\_exp}^{ij}$ should have at least P input points (i.e., one input point in each segment) to provide a sufficient condition for solution.

Once h_b and h_w are determined, the workpiece temperature distribution can be calculated using the transient thermal FEA. The heat flux h_b is directly applied using the advection concept (Fig. 2.1) and kept constant during the drilling process. The heat flux h_w in each depth segment is applied at its corresponding time step, e.g., h_w^{13} is applied on Segment #1 at the time step 3. Note the h_w in each segment is constant over the time step.

The advantage of this approach is being able to solve the temporal and spatial distributions of heat flux on HWS, particularly the sudden heat flux rise or drop, based on segment inputs. However, it may become difficult for a fairly deep hole case since many thermocouples are needed to achieve desired spatial distribution. Thus, an alternative approach, particularly for a deeper case, is proposed in the next section to solve h_w in deep hole drilling using fewer thermocouple inputs.

2.2.4 Determination of h_w - Approach #2

Approach #2 considers h_w as a moving heat source along with the drill penetrating into workpiece. The spatial distribution of h_w at a specific time t is described as $h_w(x,t)$ where x is the axial position from the drill cutting edge, as shown in Fig. 2.5. Four control points, denoted as CP1, CP2, CP3 and CP4 with their positions x_1, x_2, x_3 and x_4, respectively, determine the spatial distribution of $h_w(x,t)$. At the next time step, the heat flux value at four control points varies to change the distribution of h_w.

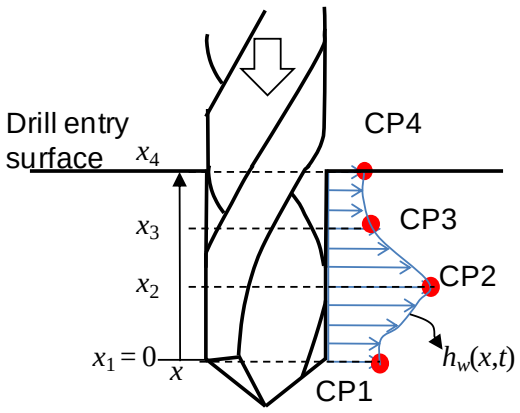

Figure 2.5 The control points to determine the heat flux spatial distribution on HWS

The position of CP4, x_4, is the drilling depth which increases with time. Since it is always the end point of $h_w(x,t)$, the change of heat flux is relatively small, thus the value of heat flux at CP4 is set as a constant. The positions of the other three points (x_1, x_2 and x_3) are fixed in this study. CP1 is the start point where $x_1 = 0$. CP2 and the location of x_2 determine the peak value of h_w. CP3 adjusts the shape of heat flux distribution between CP2 and CP4.

Before the drill reaches the depth to include CP1, CP2 and CP3, the control points are activated sequentially as shown in Fig. 2.6. In Fig. 2.6(a), at the start of drilling with $x_4 \leq x_2$, the shape of heat flux is assumed uniformly distributed. When the drilling depth exceeds the position of CP2 (i.e., $x_4 > x_2$), as shown in Fig. 2.6(b), CP1 and CP2 are activated simultaneously. CP3 is activated and form a shape as in Fig. 5 when the drilling depth exceeds x_3.

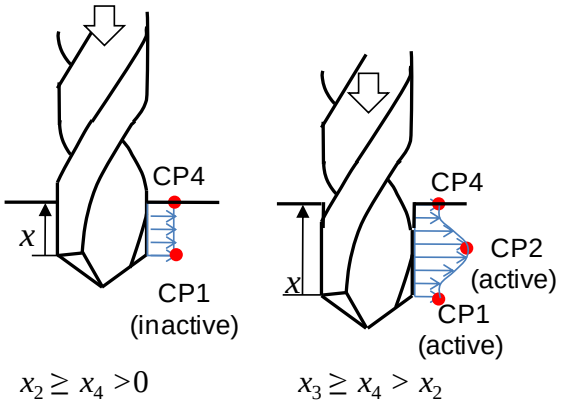

Figure 2.6 The sequence to activate the control points: (a) stage 1 when $x_2 \geq x_4 > 0$ and (b) stage 2 when $x_3 \geq x_4 > x_2$

Generally, the heat flux values of control points increase with the drill position in depth due to increasing heat generation. In this study, the heat flux value of control point is modeled as a quadratic function of time:

$$\begin{aligned}
&\text{CP4}: h_w(x_4,t) = c_0 \\
&\text{CP3}: h_w(x_3,t) = c_0 + c_{31}(t-t_3) + c_{32}(t-t_3)^2 \text{ for } t > t_3 \\
&\text{CP2}: h_w(x_2,t) = c_0 + c_{21}(t-t_2) + c_{22}(t-t_2)^2 \text{ for } t > t_2 \\
&\text{CP1}: \ h_w(x_1,t) = c_0 + c_{11}(t-t_2) + c_{12}(t-t_2)^2 \ \text{ for } t > t_2
\end{aligned} \tag{2.5}$$

where c_0 defines the initially uniform distributed h_w. Time t_2 and t_3 are the time when the drilling depth reaches x_2 and x_3, respectively. The spline function of $h_w(x,t)$ at a given time is determined by the piecewise cubic Hermite interpolation of control points.

During drilling, $h_w(x,t)$ is input to the FEA model at the corresponding time step and drill position to calculate the temperature in the workpiece. Using the generated temperature profile at the input points, T_w^i, the seven unknown coefficients (c_0, c_{11}, c_{21}, c_{31}, c_{12}, c_{22}, and c_{32}) in Eq. (2.5) can be determined by minimizing the objective function of Eq. (2.4). In addition, to reduce the computational time, the advection process (element removal) was not applied in iterations, i.e., the material to be removed by drilling was assumed already removed initially in the model. This is because this section of material has minimal effect on h_w and the computation time can be saved significantly.

2.3 Experimental design and setup

An experimental study using a 10 mm diameter and 220 mm long solid carbide drill with 140° point angle (Titex, Model A6785TFP-10) was conducted to verify the inverse method. A hole, 120 mm in depth, was drilled in the center of the cylindrical workpiece, 40 mm in diameter and 150 mm in length. The work-material is ductile iron grade 80-55-06 with 7000 kg/m^3 density, 24.2 W/m-K thermal conductivity, and 506 J/kg-K specific heat. The experimental setup is shown in Fig. 2.7. Five Type E

thermocouples (OMEGA Engineering Inc.) with 0.127 mm wire diameter were embedded in the workpiece at positions corresponding to Fig. 4 with a = 21 mm, b = 8.4 mm, and c = 10.5 mm. The thermocouple hole was 1.2 mm in diameter and filled with high thermal conductivity paste to minimize the thermal contact resistance. Two additional thermocouples, marked as A and B, were embedded to validate the temperature distribution. Thermocouple A was embedded midway between Input Points #2 and #3 with 7.5 mm from the center line, and thermocouple B was between Input Points #3 and #4 with 10.5 from the workpiece center line. The workpiece was clamped to a drilling dynamometer (Model 9272 of Kistler) and the thrust force and torque were recorded during drilling at a 1000 Hz sampling rate. The temperatures were recorded at a 100 Hz sampling rate.

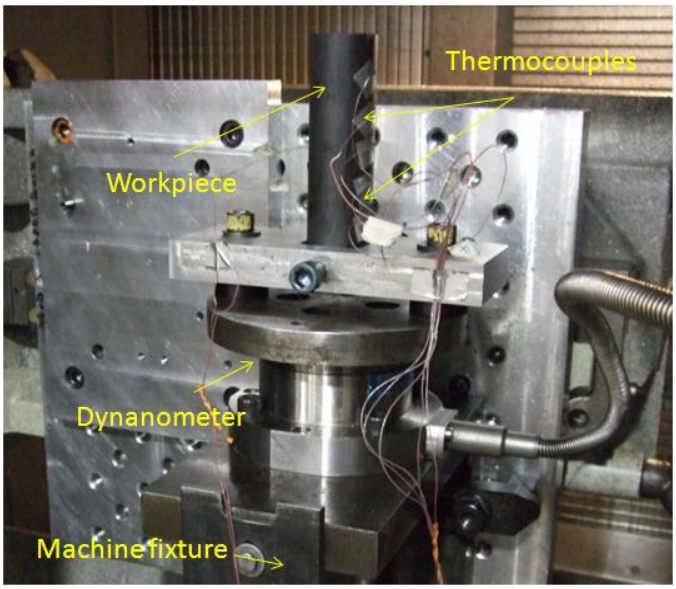

Figure 2.7 Experimental setup on Cross Hüller machine

The MQL flow rate was 50 mL/h using a Bielomatik (Neuffen, Germany) dual-channel through tool MQL delivery system on a Cross Hüller horizontal machining center at the Ford Advance Manufacturing Technology Development (AMTD) Laboratory. Dry machining was also tested to verify the heat flux from cutting edge since it can be calculated from the cutting edge geometry, thrust force, and torque under dry condition. The experimental conditions are summarized in Table 2.1.

Table 2.1Experiment conditions for deep-hole drilling

Condition	MQL	Dry
Machine	Cross Hüller SPECHT 500D	Cincinnati HMC-400EP
Drilling depth (mm)	120	105
Spindle speed (rpm)	1600	1600
Feed rate (mm/rev)	0.15	0.1

2.4 Results of heat flux on HBS

2.4.1 Solution of h_b and T_b under MQL condition

Using the measured temperature data at Input Point #1 and Eq. (2.2), the h_b (= k) is 2.90 MW/m^2 under MQL condition. The FEA-calculated T_b^i at five input points using obtained h_b is shown in Fig. 2.8. An agreement can be observed in the temperature rising region for each input point. The discrepancy after the peak temperature between T_b^i and T^i is T_w^i, which is used to solve the h_w in Sec. 2.5.

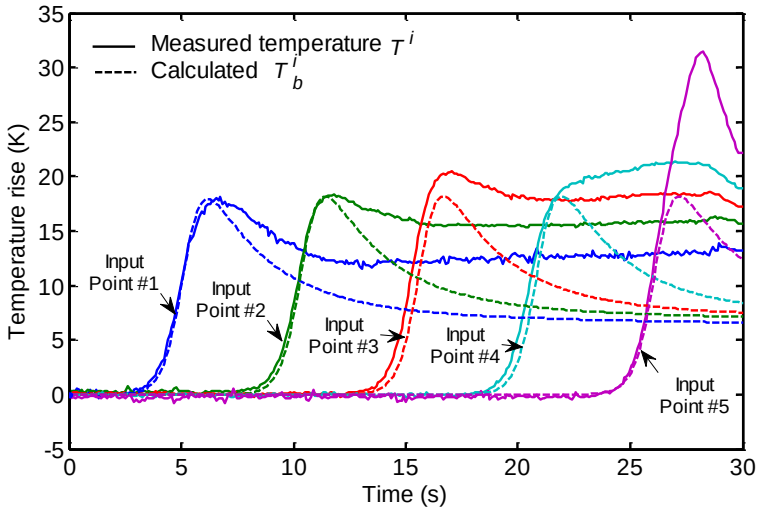

Figure 2.8 Measured temperature and calculated T_b at five input points under MQL condition

2.4.2 Validation of h_b through dry drilling

The h_b in dry drilling can be theoretically calculated based on the drill geometry and measured torque and thrust force [12]. The proposed inverse method for determining h_b is validated under a dry drilling condition by comparing with the theoretical calculation. By dividing the drill tip cutting edge into several elemental cutting tools (ECT), the heat flux applied into the workpiece by each ECT can be expressed as [12]:

$$q_{wp} = \frac{(1-\frac{q_{friction}}{q})(T_z\omega + F_z V_f)}{\pi(r_{outer}^2 - r_{inner}^2)} \tag{2.6}$$

where $q_{friction}$ is the heat generated by friction between tool and chips, q is the total amount of heat generated by each ECT, $\pi(r_{outer}^2 - r_{inner}^2)$ is the area cut by each ECT, and F_z and T_z are measured thrust force and torques on each ECT, respectively. The cutting edge was divided into seven ECTs. The heat flux calculated using Eq. (2.6) for each ECT is shown in Fig. 2.9, where r/R is the dimensionless radial position to the drill center. The dashed line in Fig. 2.9 is h_b = 6.23 MW/m^2, which is calculated using the inverse method of this study. The assumption of constant h_b on HBS matches well to the average of the theoretical calculation and validates the proposed approach.

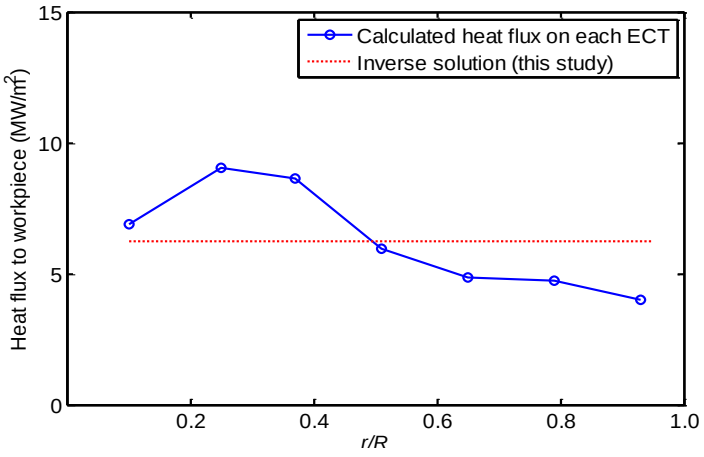

Figure 2.9 Comparison of inverse solution and calculated heat flux from each ECT

2.5 Results of heat flux on HWS

2.5.1 Solution of h_w using Approach #1

To solve h_w using Approach #1, the total hole depth was divided into five segments and 80 equal time steps of 0.375 s. The impact tensor I in Eq. (2.3) was calculated using the transient thermal FEA. As shown in Fig. 2.10(a), I_{ij11} is the temperature response of input points to the unit heat flux applied on Segment #1 at time step 1. For q >1, I_{ij1q} can be estimated by shifting the results of I_{ij11} by (q−1) time steps. An example for q=10 is shown in Fig. 2.10(b). The entire impact tensor can be estimated by this shifting technique after solving I_{ij11}, I_{ij21}, I_{ij31}, I_{ij41}, and I_{ij51}.

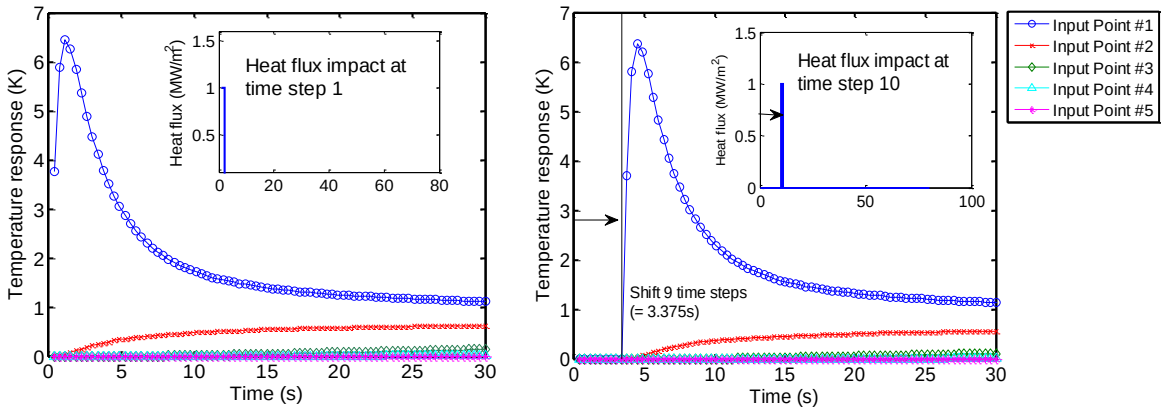

(a) (b)

Figure 2.10 Impact tensor (a) I_{ij11} calculated by transient FEA and (b) I_{ij1q} (q = 10) calculated by shifting the response results of I_{ij11}.

For a known I, h_w^{pq} can generate the temperature at five input points using Eq. (2.3). With the calculated T_w^{ij} and the experimentally measured $T_{w\_exp}^{ij}$, the inverse solution of h_w^{pq} can be solved using the objective function of Eq. (2.4). The constraints for the optimization were set to h_w = 0 for the time step before the drill enters the segments in order to reduce the amount of unknowns and to accelerate the convergence of the process. Results of h_w in MQL drilling at five segments and 80 time steps are shown in Fig. 2.11. The notable increase of h_w at Segment #5 implies a critical depth at which the chip evacuation becomes significant. This is further confirmed by examining the measured torque, shown in Fig. 2.12. At the end of drilling (Segment #5), the rapid

increase of torque is evidence of increasing friction caused by chip clogging, which is commonly observed in deep hole drilling. The rise in torque in Segment #5 causes the sharp increase of h_w in Fig. 2.11.

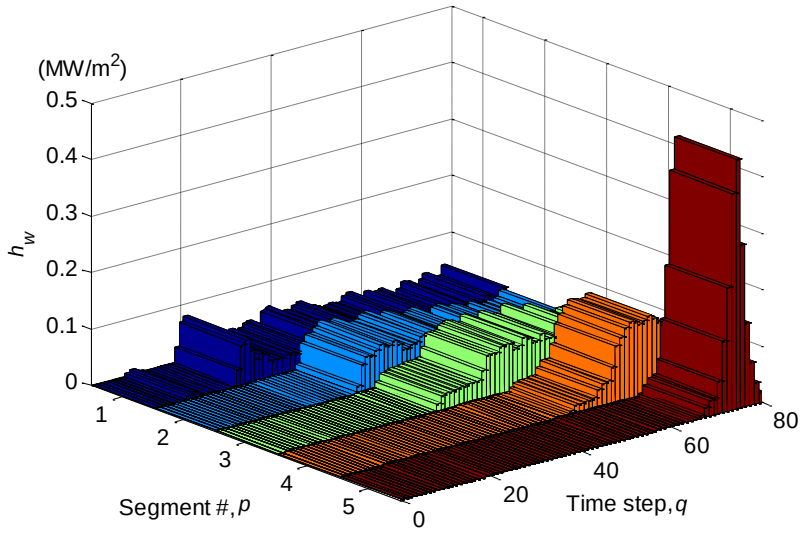

Figure 2.11 Results of inverse solution on h_w

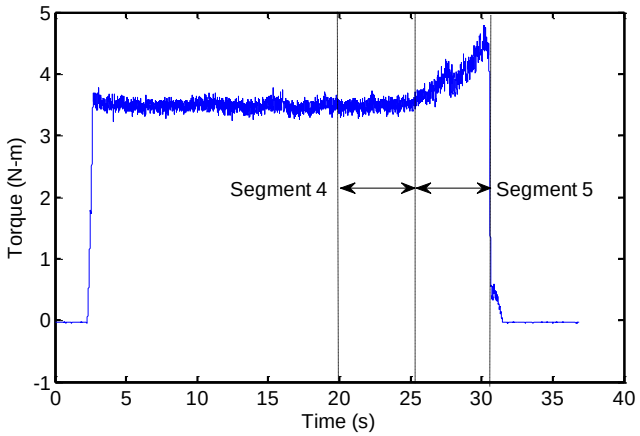

Figure 2.12 Torque data from an MQL deep hole drilling test

The inverse solution of h_w was validated in Fig. 2.13 by comparing the experimentally measured data at two validation points A and B (defined in Sec. 2.3) with the calculated temperatures via advection FEA model using the h_w and h_b as inputs. The good agreement of measured and calculated temperatures further validates the proposed approach for MQL deep hole drilling workpiece temperature analysis.

This approach can accurately predict the rapid temperature rise at Input Point #5, as shown in Fig. 2.13. As shown in the next section, Approach #2 does not have the spatial and temporal resolution to make such accurate prediction.

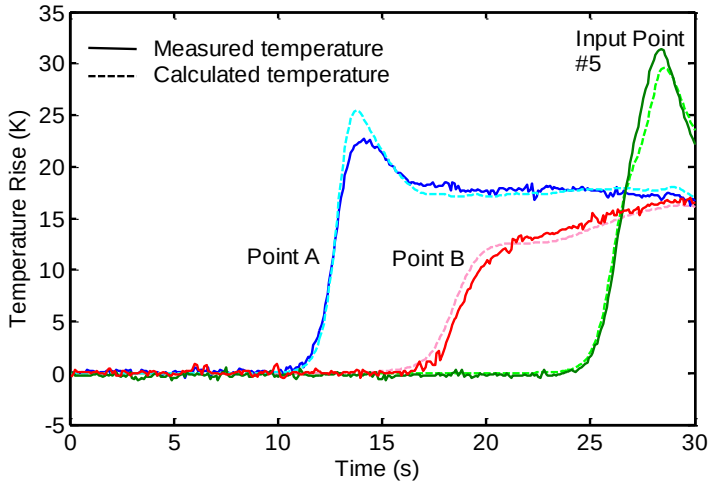

Figure 2.13 Temperature validation at points A and B using Approach #1

2.5.2 Solution of h_w using Approach #2

In Approach #2, at least three input points are needed to solve the seven coefficients (c_0, c_{11}, c_{21}, c_{31}, c_{12}, c_{22}, and c_{32}) in Eq. (2.5). In addition, these input points should be allocated at the beginning, middle and end of the target depth in order to reflect the heat flux change during the entire process. In this study, Input Points #1, #3 and #4 were selected since #5 was too close to the end of drilling depth and had limited data points. Solutions obtained by all five input points were also presented to compare with those from three input points.

To solve the optimization problem, positions of CP2 and CP3 (x_2 and x_3) need to be defined first. A proper selected position of CP2 is important when fitting the temperature profile $T_{w\_exp}{}^i$ in the optimization solution. For a given $T_w{}^i$ at certain input point, the increasing rate of temperature ($\mathrm{d}T_w{}^i/\mathrm{d}t$) starts to decrease when the maximum of h_w passes that input point. Thus, the peak value position of the derivative of $T_{w\_exp}{}^i$ can be used to estimate the corresponding x_2. In this study, the optimal x_2 was found at the

nodal point x = 13.5 mm, which yielded the peak value positions close to those from $T_{w\_exp}^{\ i}$ for i =1, 2, 3, 4 and 5; this further affirms the hypothesis of constant x_2.

CP3 was set at x_3 = 26 mm to control the curvature between CP2 and CP4. Equation (2.5) was rewritten as the function of time step q, with a total of 80 steps within 30 s machining time (0.375 s for each time step). CP2 and CP3 were activated at 10th and 18th time step (15 mm and 27 mm in drilling depth), respectively. The spline function to describe the heat flux shape at time step q, $h_w(x,q)$, was automatically generated in MATLAB with given control point values.

The initial value c_0 was set as an optimization parameter. The value of c_0 is sensitive to the convergence of the solution for the other six unknown parameters, c_{11}, c_{21}, c_{31}, c_{12}, c_{22}, and c_{32}. The optimization result showed that c_0 = 0.01 yielded the minimum objective function, among the values of 0, 0.01, 0.02, and 0.03.

The optimized variables from five and three inputs are both listed in Table 2.2, where $\sum Err$ is the summation of temperature discrepancy between $T_{w\_exp}^{\ i}$ and calculated $T_w^{\ i}$ at all five input points. The solution of five inputs had smaller $\sum Err$ in comparison to the solution of three inputs because all five inputs were considered in the optimization. Despite different coefficients and $\sum Err$, the overall heat flux distribution and growth, as shown in Fig. 2.14, are similar in both conditions. The dash lines indicate the positions of CP2 (x_2) and CP3 (x_3). The heat flux value of CP2 is the peak and increases steadily as the drill penetrates into the workpiece.

Table 2.2 Calculated coefficients of changing rates of control points

Input Points	c_{11} ($\times 10^{-2}$)	c_{21} ($\times 10^{-2}$)	c_{31} ($\times 10^{-2}$)	c_{12} ($\times 10^{-4}$)	c_{22} ($\times 10^{-4}$)	c_{32} ($\times 10^{-4}$)	$\sum Err$ (K)
#1, #2, #3, #4, #5	0.085	0.110	0.240	−0.176	0.183	−0. 185	134.6
#1, #3, #4	0.023	0.065	0.216	0.155	0.282	−0.114	149.1

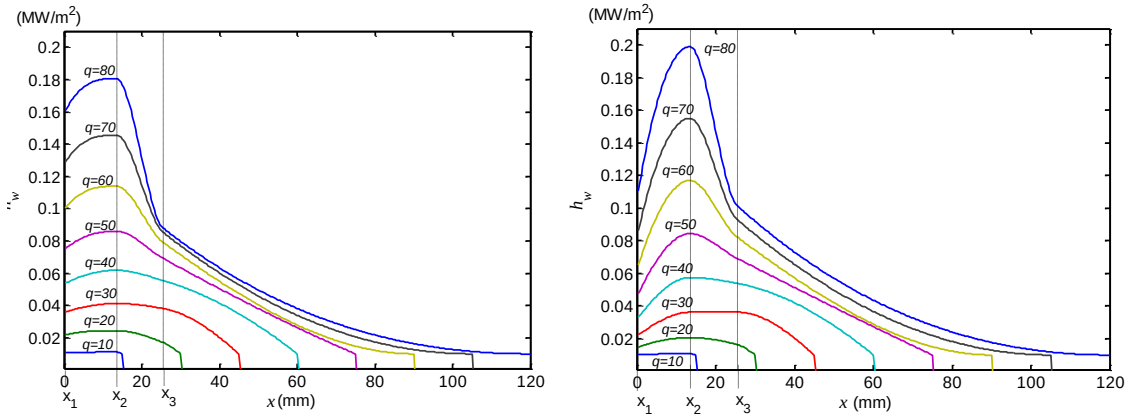

Figure 2.14 Heat flux change on HWS by applying inverse solutions from (a) five input points and (b) three input points

Figure 2.15 shows the predicted temperatures at validation points A and B and Input Point #5 by using h_b and $h_w(x,q)$ as inputs. The predicted data shows good agreement with the measured results. Results are also similar between solutions of five and three inputs. The discrepancy at Input Point #5 is due to the significant heat flux change in a short time, as the torque data shown in Fig. 2.12, which cannot be reflected on the smoothly growing heat flux function in Eq. (2.5). Therefore, although this method can achieve accurate prediction of temperature distribution by using fewer input points, it loses its spatial and temporal accuracy when the cutting process encounters a rapid change, such as the chip clogging in Segment #5 at the end of this deep hole drilling.

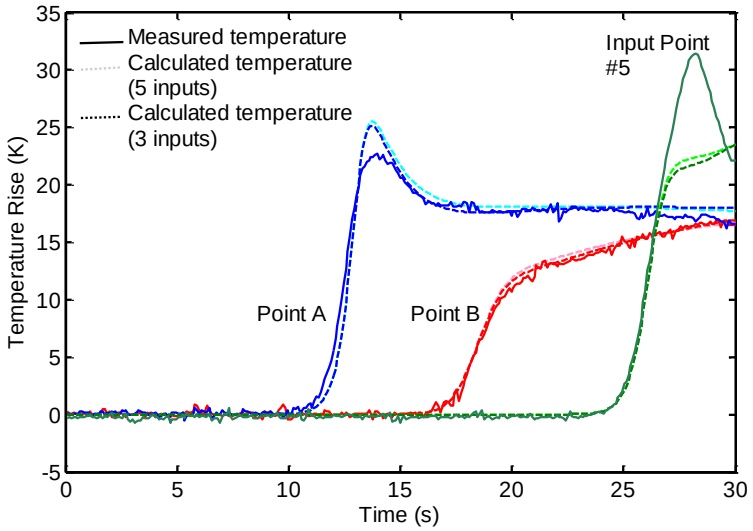

Figure 2.15 Temperature validation at points A and B using Approach #2

2.6 Workpiece temperature distributions

Figure 2.16(a) shows the workpiece temperature distribution in every 20 time steps using the solution considering only HBS (i.e., h_b). Figure 2.16(b) show the workpiece temperature calculated from the inverse solution (h_b and h_w) using either Approaches #1 or #2, which have almost the same temperature results. HBS is considered as the main and only heat source in previous drilling thermal modeling of workpiece. This study shows that the heat flux on HWS significantly increases the workpiece temperature as the time step increases. The average temperature over the entire model is about 10°C higher when HWS is considered in addition to HBS. Furthermore, although the surface temperature of workpiece (right edge of the model) is in the same level in Fig. 2.16, the temperature close to the drilled holed is much higher in the case when HWS is considered (Fig. 2.16(b)). This implies that the conventional temperature measurement on workpiece surface, such as infrared camera, may overestimate the stability and neglect potential dimensional errors.

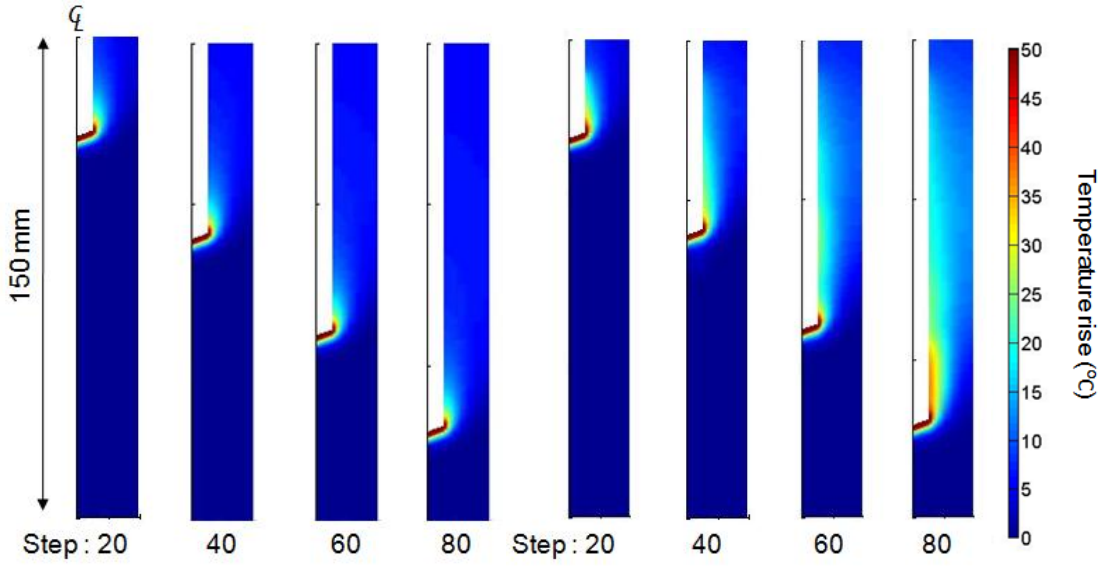

(a) **(b)**

Figure 2.16 Temperature distribution of the workpiece under MQL condition by considering heat from (a) HBS, (b) HBS and HWS (Approach #1 or #2 with five input points)

Figure 2.17 shows the heat power (the heat flux times the applied area) on HBS and HWS calculated from h_b and $h_w(x,q)$ in Sec. 2.5.2, respectively. The h_w is usually neglected in thermal modeling of shallow hole drilling. This is true as indicated in Fig. 2.17 that HWS has limited effect when the drilling depth is 30 mm (3 times the drill diameter). As the drilling depth increases, the heat power on HWS becomes more significant. At the drilling depth of 120 mm (12 times the drill diameter), the HWS heat power is almost equal to that from HBS. This implies that, if the drilling continues, HWS will have a significant effect on the workpiece temperature and the associated hole distortion.

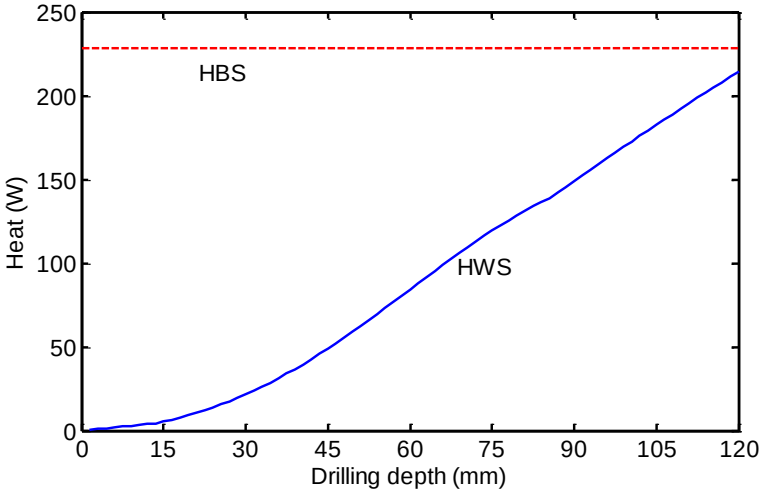

Figure 2.17 The comparison of heat power varying with drilling depth on HBS and HWS

2.7 Conclusions

In this study, the temporal and spatial distributions of heat flux on the hole wall surface, h_w, in deep drilling was determined using the inverse heat transfer method. In deep hole drilling, the contribution of h_w to the workpiece temperature was found significant under MQL condition compared to that of hole bottom surface (HBS) and not negligible in the thermal analysis of deep hole drilling. Results in this study show the heat absorbed via HWS into workpiece was close to HBS when the drilling depth is 12 times

the drill diameter, and it will be larger and contributes more significantly to workpiece temperature in a deeper drilling position.

Two approaches proposed to define h_w are trade-off between the number of inputs and the capability of reflecting sudden heat flux change. Approach #1 demonstrated to be useful for the drilling process with chip clogging at the cost of requiring many thermocouple input points to reach an acceptable spatial resolution in a deep hole drilling case. Approach #2 was developed to reduce the number of thermocouples required to determine the heat flux distribution of h_w. The limit of this approach was observed with chip clogging during deep hole drilling workpiece temperature analysis. Approach #2 will require further advancement on this aspect.

Using the proposed inverse heat transfer method, future research will concentrate on studying the heat generation of HWS for different MQL drilling parameters, drill geometry, drilling depth and cutting fluids. Another goal of this study is to accurately predict the hole and workpiece dimensional errors caused by thermal distortion in deep-hole drilling in order to optimize the process parameters and design the drill geometry.

References

[1] Stoll, A., Sebastian, A.J., Klosinski, R., and Furness R., 2008, "Minimum Quantity Lubrication (MQL) is a Key Technology for Driving the Paradigm Shift in Machining Operations," SAE Paper 01-1128.

[2] Filipovic, A. and Stephenson, D., 2006, "Minimum Quantity Lubrication (MQL) Application in Automotive Powertrain Machining," Machining Science & Technology, 10, pp. 3-22.

[3] Heinemann, R., Hinduja, S., Barrow, G., and Petuelli, G., 2006, "Effect of MQL on the tool life of small twist drills in deep-hole drilling," International Journal of Machine Tools and manufacture, 46, pp. 1-6.

[4] Liao, Y. S. and Lin, H. M., 2007, "Mechanism of minimum quantity lubrication in highspeed milling of hardened steel," International Journal of Machine Tools and Manufacture, 47, pp. 1660-1666.

[5] Autret, R. and Liang, S. Y., 2003, "Minimum quantity lubrication in finish hard turning," HNICEM '03.

[6] Silva, L.R., Bianchi, E.C., Catai, R.E., Fusse, R.Y., and Franca, T.V., 2005, "Study on the behavior of the minimum quantity lubricant - MQL technique under different lubricating and cooling conditions when grinding ABNT 4340 steel," Journal of the Brazilian Society of Mechanical Sciences and Engineering, 27(2), pp. 192-199.

[7] Stephenson, D. A. and Agapiou, J. S., 2006, Metal Cutting Theory and Practice, 2nd Edition, Taylor and Francis, Boca Raton, FL.

[8] Agapiou, J. S. and Stephenson, D. A., 1994, "Analytical and experimental studies of drill temperature," Transactions of the ASME, 116, pp.54-60.

[9] Bono, M. and Ni, J., 2006, "The location of the maximum temperature on the cutting edges of a drill," International Journal of Machine Tools & Manufacture, 46, pp.901-907.

[10] Li, R. and Shih, A. J., 2007, "Tool temperature in titanium drilling," Journal of Manufacturing Science and Engineering, 129, pp. 740-749.

[11] Bono, M. and Ni, J., 2001, “The effects of thermal distortions on the diameter and cylindricity of dry drilled holes,” International Journal of Machine Tools and Manufacture, 41, pp.2261-2270.

[12] Bono, M. and Ni, J., 2002, “A model for predicting the heat flow into the workpiece in dry drilling,” Journal of Manufacturing Science and Engineering, 124, pp. 773-777.

[13] Ke, F., Ni, J., and Stephenson, D. A., 2005, “Continuous Chip Formation in Drilling,” International Journal of Machine Tools and Manufacture, 45(150), pp. 1652–1658.

[14] Li, R. and Shih, A. J., 2007, “Finite element modeling of high-throughput drilling of Ti-6Al-4V,” Transactions of NAMRI/SME, pp. 73-80.

[15] Papalambros, P. Y. and Wilde, D. J., 2000, Principles of Optimal Design: Modeling and Computation 2nd Edition, Cambridge University Press, NY.

CHAPTER 3

INVESTIGATION OF AIR PRESSURE AND FEED RATE EFFECTS ON WORKPIECE TEMPERATURE IN MQL DEEP HOLE DRILLING USING THE INVERSE HEAT TRANSFER METHOD

ABSTRACT

This research studies the workpiece temperature in deep-hole drilling with through tool minimum quantity lubrication (MQL) technique under different air pressures and feed rates. A modeling approach based on the inverse heat transfer method is developed to quantify the heat flux as function of time and drill position in drilling deep holes with aspect ratio of 20. An air pressure of 500 and 1000 kPa along with two feed rates, 240 and 480 mm/min, were tested for comparison in drilling 200 mm deep holes on ductile iron using a 10 mm diameter carbide drill. Chip accumulation and clogging occurred in the case of slow feed rate and low air pressure, and the maximum heat flux generated on the hole wall surface (HWS) was about 100 times larger than that under a smooth chip evacuation condition in all other cases. Although higher air pressure can eliminate the chip accumulation during the slow feed rate case and reduce the workpiece temperature, it does not provide any further improvement in the high feed rate case. Based on the temperature modeling results, the thermal energy absorbed through HWS is significant in MQL deep-hole drilling. The heat flux on HWS contributes around 25% of the total workpiece temperature rise in a smooth chip evacuation condition, and up to 66% in a chip accumulation condition.

Contents of this chapter have been submitted as Tai, B.L., Stephenson, D.A., White, S.B., and Shih, A.J., (2011), "Investigation of air pressure and feed rate effects on workpiece temperature in MQL deep hole drilling using the inverse heat transfer method," *International Journal of Machine Tools and Manufacture*

3.1 Introduction

Minimum quantity lubrication (MQL) machining is a near-dry process which applies a minute amount of straight-oil lubricant mixed with compressed air to the tool-workpiece interface. This technique has been steadily implemented in automotive powertrain machining operations. MQL has demonstrated to have equal or better performance in many experimental tests, such as milling, turning and drilling [1-4]. However, MQL application in deep-hole drilling is still technically challenging due to the high tool and workpiece temperature generated in the cutting process.

Deep-hole drilling refers to a hole depth to diameter aspect ratio larger than 10, and is a key machining process for oil gallery holes in engine block, oil holes in crankshaft, and valve body spool bores in automotive powertrain manufacturing. Although MQL has better lubrication than water-based metal working fluid [5], cooling and chip evacuation are barriers in deep-hole drilling applications. The resulting elevated temperature around cutting zone can cause the thermal damage on the drill, chip build-up, hole distortion and entire part distortion. The chip accumulation and clogging, common problems in dry deep-hole drilling [6], are more severe under MQL condition compared to flood cooling. Since chips contain most of the heat produced during drilling [7], improper chip evacuation can cause a large amount of heat to flow into workpiece, resulting in part dimensional errors. Increased air pressure is one solution applied in industry to overcome the chip clogging problem. Hussain et al. [8] concluded that higher cutting speed, feed rate, air pressure and oil delivery can generate lower workpiece temperature. Agapiou [9] reported that the lower workpiece temperature in compacted graphite iron (CGI) gun-drilling can be achieved by higher feed and air pressure as well as better drill point design. To further understand the effect of these factors, this study aims to quantify the heat generation and estimate the workpiece temperature in deep hole drilling under different feed rates and air pressures with the dual-channel MQL delivery system commonly used in production.

Thermal modeling of the drilling process has been studied extensively and reviewed in [7,10,11]. Most of the thermal models are focused on the drill temperature; however, very few studies investigate the workpiece temperature. Fleischer et al. [12] used the steady-state workpiece temperature after drilling to estimate the average surface

heat flux over time. However, assumptions of the constant machined area and heat flux are not suitable for deep-hole drilling. An advection model, proposed by Bono and Ni [13], calculates the heat flux flowing to the workpiece based on the torque, force and drill geometry. This model enables step-by-step heat flux supply to estimate the temperature distribution at each time step. To apply this model for MQL deep-hole drilling, the heat flux, influenced by material removal, friction, compressive air and high temperature chips in deep hole drilling, needs to be estimated first. Tai et al. [14] has developed an inverse heat transfer method to determine the heat fluxes on the drilled hole bottom surface (HBS) and the hole wall surface (HWS) based on temperatures measured using thermocouples embedded in the workpiece. The heat fluxes are applied to calculate workpiece temperature distributions.

To accurately find the temporal and spatial distribution of heat flux on HWS in MQL deep hole drilling is the key development of this study based on the inverse heat transfer method. The approach using control points with their heat flux changing as a quadratic function of time to estimate the HWS heat flux has been developed and verified in deep holes with aspect ratio of 12 [14]. This control-point approach is further advanced in this study to analyze the heat fluxes in drilling deeper holes with aspect ratio greater than 20 under different chip evacuation conditions affected by air pressure and feed rate.

In this paper, the inverse heat transfer method is reviewed and an advanced approach is described in Sec. 3.2. The experimental design and the experimentally measured data, including temperature and torque, are presented in Sec. 3.3. This is followed by the discussion of HBS and HWS heat fluxes, workpiece temperature distributions and heat partition analysis for the four MQL drilling conditions in Sec. 3.4.

3.2 Heat flux in deep-hole drilling

Two heat fluxes on the workpiece during deep-hole drilling are defined as h_b on HBS and h_w on HWS. The workpiece temperature distribution can be calculated by applying these two heat fluxes in the finite element analysis (FEA) of the workpiece model. A review of the inverse heat transfer method to determine heat fluxes and an advanced approach using control points to estimate h_w are presented in this section.

3.2.1 Review of inverse heat transfer method in MQL deep-hole drilling

The inverse heat transfer method for MQL deep hole drilling uses an optimization algorithm to search for h_b and h_w that minimize the objective function of the discrepancy in FEA calculated and experimentally measured workpiece temperature at specific thermocouple locations [14]. The axisymmetric FEA mesh of the cylindrical workpiece with length *l*, diameter *w* and hole (or drill) diameter *D* is shown in Fig. 3.1.

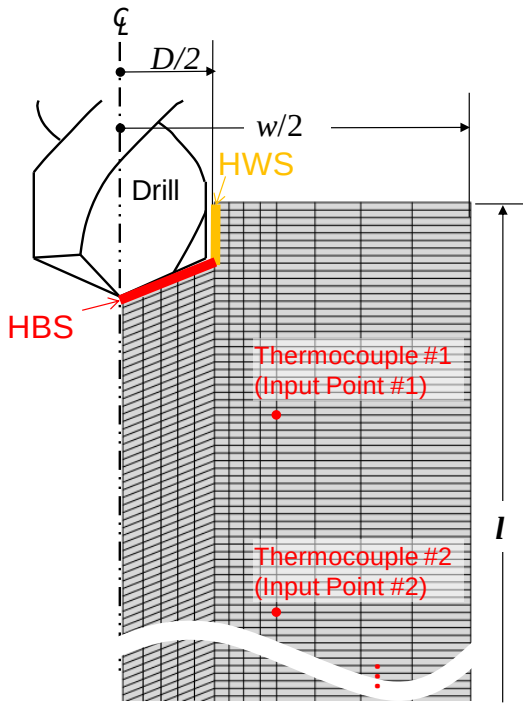

Figure 3.1 Hole wall surface (HWS), hole bottom surface (HBS) and the 2-D axisymmetric finite element mesh

The advection model [13] was adopted to mimic the material removal as the drill penetrated into the workpiece. It is achieved by removing a layer of five elements located along the HBS at each time step and applying the h_b to the subsequent layer of five elements. The h_w is described as the function of both time and nodal position along the depth and applied on the HWS. The workpiece model temperature then can be calculated. The experimentally measured temperature data are obtained by thermocouples embedded in the workpiece along the hole depth and close to the hole. These thermocouples are defined as Input Points since they are the inputs of the inverse heat

transfer method. The temperature rise at Input Point *i* in the workpiece is assumed to be the superposition of the temperature rise T_b and T_w caused by h_b and h_w, respectively.

The h_b is assumed time-independent and uniformly distributed, thus T_b would be proportional to h_b. By fitting the temperature at Input Points, h_b and T_b can be first obtained. The solution of h_b has been verified to be around the average of theoretically calculated heat flux distribution on the cutting edge based on torque, thrust force and drill geometry [14]. The discrepancy between measured temperature T and T_b is T_w, which is used to estimate the temporal and spatial change of h_w.

An approach developed in our previous study [14] estimates the h_w by interpolating through control points (CPs), as illustrated in Fig. 3.2. The number of Input Points needed in this approach is independent of the hole depth, thus it is suitable for a fairly deep hole. The challenge of this control point approach is to model the heat flux as the function of time to create the temporal distribution of h_w. A quadratic time function has been investigated in our previous study [14]. This quadratic time function was not adequate for analyzing the drilling of deep holes with aspect ratio of 20 in this study. Therefore, an advanced CP approach is explored in the next section.

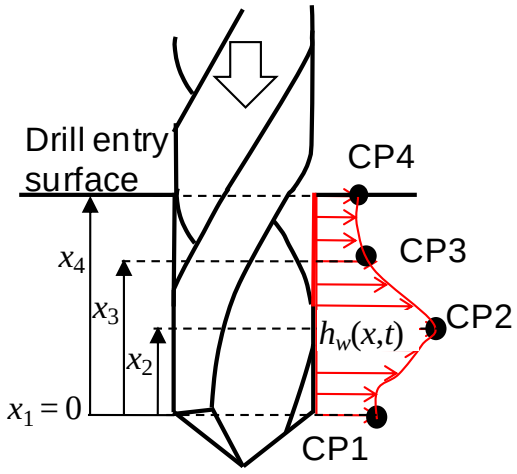

Figure 3.2 The control points to determine the heat flux spatial distribution on HWS

3.2.2 Control point approach for determining h_w

In the control point approach, the spatial distribution of h_w is determined by four CPs, denoted as CP1, CP2, CP3, and CP4 in Fig. 3.2. Adding more CPs can describe h_w

more accurately; however, it also increases the unknown variables for the optimization algorithm to find the heat flux for each CP. As shown in Fig. 3.2, CP1 is the start point where x_1=0, and CP4 is the end point where x_4 is the drilled hole depth, which is a function of drilling time. CP2 is the peak of the heat flux distribution located at x_2. It is about 1.5 times the hole diameter from HBS, determined based on the derivative of T_w [14]. CP3 is set at $x_3 = 2x_2$ to fit the transition between CP2 and CP4.

The temporal distribution of h_w is determined by varying the heat flux of each CP with a function of time. Values of CP1 or CP3 may equal or exceed that of CP2 under extreme conditions, such as chip accumulation or clogging. The values of all control points are assumed constant in the beginning of the drilling process and start to change when HBS reaches the CP positions. For example, CP2 is activated when drilling depth reaches x_2 (or time t_2).

The change of heat flux at control points follows a specific time function, named as CP heat flux model. Two CP heat flux models, polynomial and bilinear, are studied to reflect the chip accumulation and the smooth chip evacuation condition, respectively, in deep hole drilling. Chip accumulation is when chips start accumulating but have not clogged the hole during drilling. In this case, the heat flux keeps increasing rapidly before the severe clogging occurs, as shown in Fig. 3.3(a). The CP heat flux therefore is described as a polynomial function of time, and the order of polynomial determines the ascending rate of heat flux. The mathematical expression for the polynomial CP heat flux model for h_w is:

$$\begin{aligned}
&\mathrm{CP1}: h_w(x_1,t) = c_0 + c_{11}(t-t_2) + c_{12}(t-t_2)^p \ \text{for}\, t > t_2 \\
&\mathrm{CP2}: h_w(x_2,t) = c_0 + c_{21}(t-t_2) + c_{22}(t-t_2)^p \ \text{for}\, t > t_2 \\
&\mathrm{CP3}: h_w(x_3,t) = c_0 + c_{31}(t-t_3) + c_{32}(t-t_3)^p \ \text{for}\, t > t_3 \\
&\mathrm{CP4}: h_w(x_4,t) = c_0
\end{aligned} \tag{3.1}$$

where c_0, c_{11}, c_{12}, c_{21}, c_{22}, c_{31}, and c_{32} are the unknowns, t_2 is the time to activate both CP1 and CP2, t_3 is the time to activate CP3, and p is the polynomial power which determines the ascending rate of heat flux. The p = 2 is the quadratic function used in the previous study [14] and has been verified with measured temperature data.

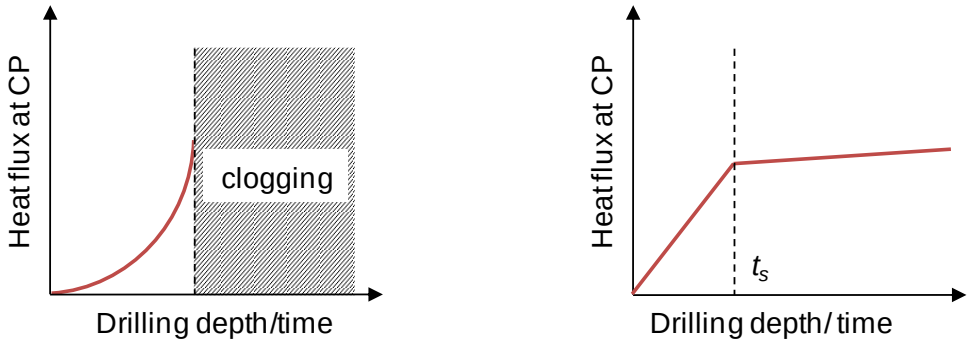

Figure 3.3 CP heat flux models to determine the temporal change of h_w: (a) polynomial model for the chip accumulation case and (b) bilinear model for the smooth chip evacuation case

For the smooth chip evacuation case, the heat flux of control points is assumed to increase linearly to a specific depth, and then either remains the same or linearly increases at a lower rate. This bilinear phenomenon is illustrated in Fig. 3.3(b). The bilinear CP heat flux model for h_w is:

$$\begin{aligned}
&\text{CP1}: h_w(x_1,t) = c_0 + c_{11}(t-t_2) \text{ for } t_2 < t < t_s \\
&\qquad h_w(x_1,t) = h_w(x_1,t_s) + c_{12}(t-t_s) \text{ for } t \geq t_s \\
&\text{CP2}: h_w(x_2,t) = c_0 + c_{21}(t-t_2) \text{ for } t_2 < t < t_s \\
&\qquad h_w(x_2,t) = h_w(x_2,t_s) + c_{22}(t-t_s) \text{ for } t \geq t_s \\
&\text{CP3}: h_w(x_3,t) = c_0 + c_{31}(t-t_3) \text{ for } t_3 < t < t_s \\
&\qquad h_w(x_3,t) = h_w(x_3,t_s) + c_{32}(t-t_s) \text{ for } t \geq t_s \\
&\text{CP4}: h_w(x_4,t) = c_0
\end{aligned} \tag{3.2}$$

where t_s is the transition time. With a given t_s in the bilinear model, seven variables (c_0, c_{11}, c_{12}, c_{21}, c_{22}, c_{31}, and c_{32}) remain to be solved by the optimization algorithm.

The flow chart that summarizes the optimization procedure to solve h_w is illustrated in Fig. 3.4. The type of CP heat flux model is first selected based on the trend observed in the experimental temperature data. Second, a set of parameters (p for the polynomial model and t_s for the bilinear model) are selected for the optimization algorithm. With a given parameter, the third step uses the sequential quadratic programming (SQP) as optimization algorithm to find the seven variables that minimize

the value of objective function, which is the summation of the discrepancy of experimentally measured T_w (denoted as T_{w_exp}) and the FEA-calculated T_w (denoted as T_{w_FEA}). The parameter then is varied and the optimization algorithm finds another optimal value of objective function. The parameter and its corresponding variables that generate the lowest value of objective function are the solution for h_w using the CP heat flux model.

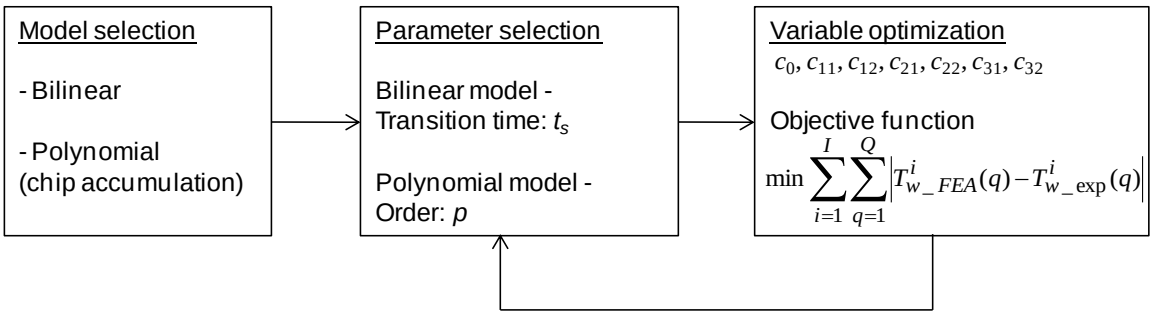

Figure 3.4 The inverse heat transfer optimization flow chart to determine h_w

To ensure the existence and uniqueness of solutions, the previous study [14] has proved that at least three input points along the depth are needed for the case of four control points with seven unknowns. Increasing the number of input points can reduce the effect of measurement errors and deviations. Therefore, five thermocouple input points (instead of three in [14]) were used in this study to ensure the accuracy of h_w.

3.3 Experiments

3.3.1 Experimental setup and design

The experiments were conducted on the EX-CELL-O horizontal machining center (Model XHC-241) using the Bielomatik (Neuffen, Germany) dual channel through tool MQL delivery system at the Ford Motor Company's Advanced Manufacturing Technology Development (AMTD) Laboratory (Livonia, MI). The cylindrical workpiece was ductile iron ASTM A536 grade 80-55-06, 40 mm in diameter and 210 mm in length. A 10 mm deep pilot hole, as illustrated in Fig. 3.5, was first drilled for guidance. A 200 mm through hole was drilled by a 10 mm diameter and 220 mm long solid carbide drill with 140° point angle (Titex, Model A6785TFP-10).

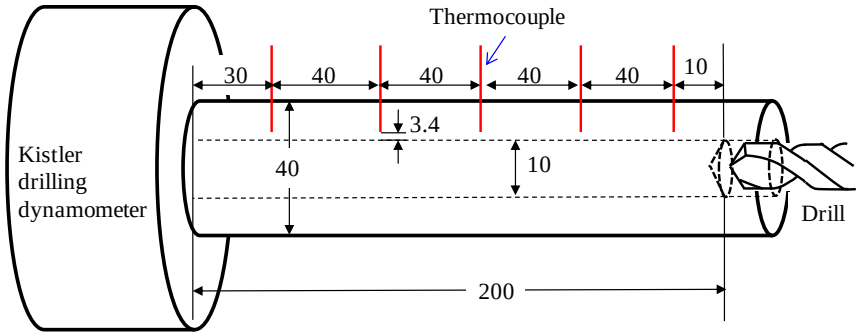

Figure 3.5 Experimental setup for MQL deep hole drilling (unit: mm)

A schematic of the experimental setup is shown in Fig. 3.5 for temperature and torque measurements. Five Type E thermocouples with 0.127 mm wire diameter (OMEGA Model 5TC-TT-E-36-72) were embedded in pre-drilled holes of 1.2 mm in diameter and filled with high thermal conductivity paste to minimize the thermal contact resistance. These pre-drilled holes were 3.4 mm from the HWS and 40 mm apart from each other. The first thermocouple is 10 mm from the beginning of deep hole drilling. The workpiece was clamped to a drilling dynamometer (Kistler Model 9272). During drilling, the thrust force and torque were measured at 1000 Hz sampling rate and temperatures were recorded at 10 Hz sampling rate.

The MQL flow rate was set at 37 mL/h, and the higher air pressure (1000 kPa or 10 bar) was achieved by an external air compressor to increase the shop air pressure (500 kPa or 5 bar). Four drilling conditions, denoted as A, B, C and D in Table 3.1, include two feed rates (240 and 480 mm/min) and two air pressures (500 and 1000 kPa). Tests A and B were under slower feed rate (240 mm/min) with 50 s drilling time. Tests C and D were under faster feed rate (480 mm/min) with 25 s drilling time. Tests A and C were under the low air pressure (500 kPa) and Tests B and D were under the high air pressure (1000 kPa).

Table 3.1 Machining parameters in the experimental study

Test #	Testing variables		Machine setting	
	Air pressure (kPa)	Feed rate (mm/min)	Feed (mm/rev)	Spindle speed (rpm)
A	500	240	0.15	1600
B	1000	240	0.15	1600
C	500	480	0.20	2400
D	1000	480	0.20	2400

3.3.2 Measured drilling torque and workpiece temperature

The torque data measured during drilling is presented in Fig. 3.6. A rapid increase of torque in Test A (slow feed rate and low air pressure) due to severe chip clogging can be observed after 75 mm of drilling. The maximum torque is over 50 N-m, more than 10 times than that in the beginning of drilling. The steady-state torque result in Test B, around 4 N-m, indicates that the 1000 kPa high pressure air eliminates the chip clogging problem in this drilling condition. Doubled feed rate in Tests C and D results in around 35% increase in torque compared to that in Test B. Despite low air pressure, no clogging phenomenon is observed in Test C due to a better chip evacuation condition generated by higher spindle speed. By comparing Tests C and D, the high air pressure cannot further lower the torque when the chips are evacuated properly.

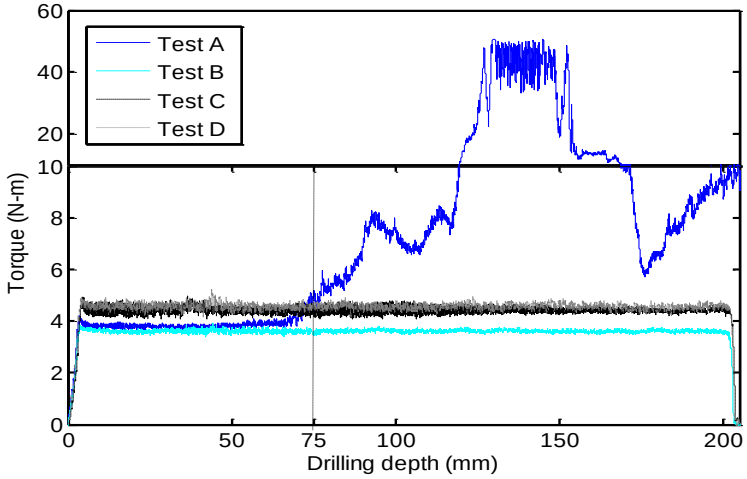

Figure 3.6 Measured torque for four drilling conditions

Temperature data at Input Points are shown in Fig. 3.7, where the profiles from left to right are Input Points #1 to #5, respectively. Data at Input Points #4 and #5 in Test A were missing since the machine slowed down and feed changed under the extreme spindle load. In Test A, similar to the phenomena observed on the torque data, the temperature increases rapidly with the increasing drilling depth. The maximum measured temperature is around 250°C at Input Point #3 (at 90 mm drilling depth). Although Tests A and B have the same torque profile before the depth of 75 mm, the temperature measurements present very different profiles at Input Points #1 and #2 (at 10 and 50 mm

drilling depth, respectively). The reason is that the chip accumulation could not be reflected on the torque data until it turns to a clogging problem. Temperature reflects the chip accumulation earlier than torque since the heat in chips transfer into workpiece via HWS. For Tests C and D, the temperature profiles (Fig. 3.7(b)) are similar to each other, and are much lower than those in Tests A and B due to the faster moving heat source as a result of higher feed rate.

The measured temperatures are used to find h_w and h_b, which will be presented in the following section.

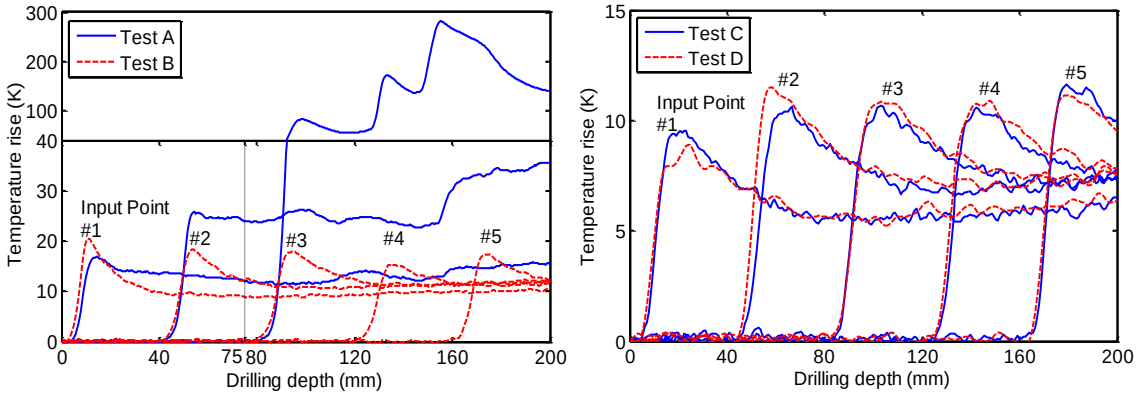

(a) (b)

Figure 3.7 Temperature data at Input Points in (a) Tests A and B and (b) Tests C and D

3.4 Thermal analysis results

The h_b, h_w, workpiece temperature and signifiance of hole wall surface heat flux for the four drilling conditions are presented.

3.4.1 Heat flux h_b

The temperature at Input Point #1, which had the least effect of h_w on measured temperature in the rising phase [14], was used to find the h_b for all four tests. Material properties of the ductile iron workpiece for FEA were 7000 kg/m^3 density, 24.2 W/m·K thermal conductivity, and 506 J/kg·K specific heat. The boundary condition was free convection with the coefficient of 10 W/m^2·K. Since Tests C and D displayed almost identical torque and temperature data (Fig. 3.7(b)), the h_b, h_w, and workpiece temperature

were about the same for these two test conditions. Results of Tests C and D were denoted as Test C/D.

The h_b was determined to be 3.25, 3.10, and 4.92 MW/m^2 for Tests A, B, and C/D, respectively. The larger h_b in Test C/D was due to the larger torque and thrust force produced by higher spindle speed and feed. The error of the actual thermocouple radial position (3.4 mm from the HWS) may result in an overestimated or underestimated h_b. In this experiment, the potential machining error for the thermocouple embedded holes is $\pm$0.2 mm, which is equivalent the maximum 10% uncertainty for h_b.

3.4.2 Heat flux h_w

In FEA of h_w, the 200 mm drilling depth was divided to 125 time steps. Since the calculated temperature, T_{w_FEA}, had less than 2% difference between 125 and 500 time steps, 125 time steps were considered adequate.

For all four tests, positions of CPs were assigned at x_2 = 14.4 mm (CP2) and x_3 = 28.8 mm (CP3). CP1 and CP4 were always located at x = 0 and the end of drilled length, respectively. The CP heat flux model and parameters for Tests A, B, and C/D are listed in Table 2. For Test A, the polynomial CP heat flux model with three Input Points (#1 to #3) was applied up to 100 mm drilling depth due to severe chip clogging problem beyond this point. The rapid and significant change of heat flux during chip clogging cannot be modeled as a polynomial model. For Tests B and C/D, the bilinear CP heat flux model was adopted since no chip clogging was observed in the torque data. The tested parameters for Test A were p = 2, 3, 4, and 5, for Tests B were t_s =24.8, 20.8, 16.8, and 12.8 s, and for Test C/D were t_s=12.4, 10.4, 8.4, and 6.4 s. These values cover a wide range for optimization the parameter. Based on the procedure in Fig. 4, results of the optimal parameters were p = 4 for Test A, t_s = 16.8 s for Test B, and t_s = 8.4 s for Test C/D.

Table 3.2 Parameter selection for optimization algorithm

Test	CP heat flux model	Tested parameters	Optimal parameter
A	Polynomial	2, 3, 4, 5 (order)	p = 4 (order)
B	Bilinear	24.8, 20.8, 16.8, 12.8 (s)	t_s = 16.8 (s)
C/D	Bilinear	12.4, 10.4, 8.4, 6.4 (s)	t_s = 8.4 (s)

Figure 3.8 shows the results of CP heat flux, FEA calculated temperatures, and the experimental temperatures at Input Points. Good agreement between the measured data and calculated temperatures validates the polynomial and bilinear CP heat flux models in the control point approach. Despite different feed rates in Tests B and D, the transition time (t_s) of CP heat flux model corresponds to the same drilling depth of 67.5 mm. The maximum h_w in Test A is fairly high (close to 3 MW/m^2 at CP1), about 100 times larger than that in Tests B and C/D (around 35 kW/m^2). This indicates that the chip accumulation significantly increases the h_w. The maximum h_w in Test D (CP2 = 35 kW/m^2) is larger than that in Test B (CP2 = 27 kW/m^2) under the same air pressure. This is likely due to the higher feed rate in Test D, compared to Test B, that generates thicker chips and higher material removal rate.

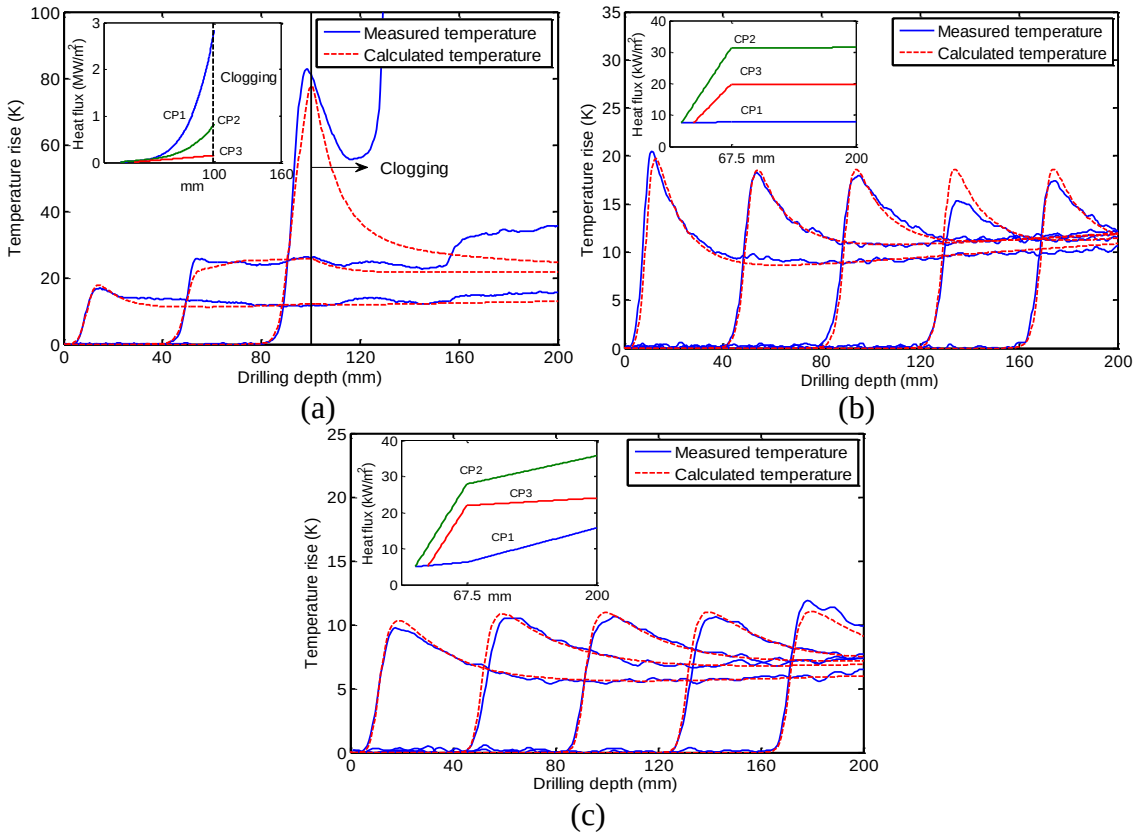

Figure 3.8 Results of CP heat flux and FEA calculated temperatures in (a) Test A (before the severe chip clogging), (b) Test B, and (c) Tests C/D

3.4.3 Workpiece temperature distributions

The workpiece temperature distribution was calculated by applying the solution of h_b and h_w in FEA advection model. Figure 3.9(a) shows four workpiece temperature distributions in Test A from 4 to 100 mm drilling depth with 32 mm increment. Figures 9(b) and (c) show seven workpiece temperature distributions in Tests B and C/D from 4 to 200 mm with the same 32 mm increment. By comparing the temperature change at 100 mm drilling depth, Test A has the most significant temperature rise due to the chip accumulation. Test C/D has the least temperature change because of the shorter drilling time and proper chip evacuation.

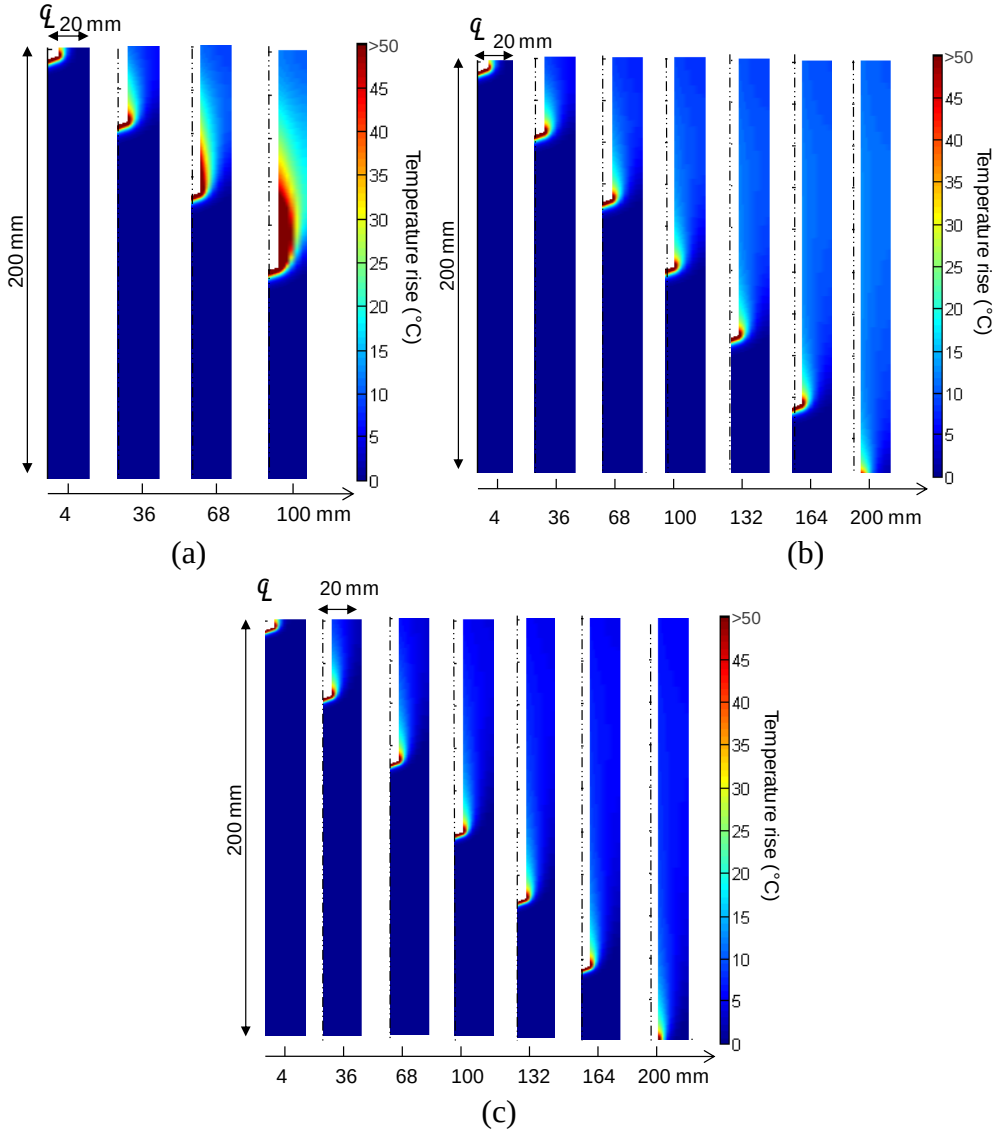

Figure 3.9 Temperature distribution in the workpiece during drilling in (a) Test A (before the occurrence of severe chip clogging), (b) Test B, and (c) Test C/D

Figure 3.10 shows the close-up view of workpiece temperature distributions around the bottom of the hole in Tests A, B, and C/D at 100 mm drilling depth. Points *e* and *f* are locations of the maximum temperature on HBS and HWS, respectively. Point *e* is located at the center of HBS in all three test conditions. The slightly larger Point *e* temperature in Test A (233.6°C) than in Test B (210.3°C) is due to the larger h_b of Test A. The Point *e* temperature is dominated by h_b since it is not affected by the significantly higher h_w in Test A. For Test C/D, despite the larger h_b (4.92 MW/m^2), the Point *e* temperature (212.5°C) is still close to that of Tests A and B, since a larger portion of h_b is removed with elements in advection model as a result of faster feed rate.

The location of Point *f* is 4.8 mm from HBS in Test A, and is at the intersection of HBS and HWS in Tests B and C/D. Point *f* is close to or at the HBS when the h_w is much smaller than h_b, such as Tests B and C/D. Since Test A has fairly high h_w and comparable to its h_b, Point *f* is away from the HBS. Furthermore, Test A has the highest temperature among all tests and is the only one having higher Point *f* temperature (244.6°C) than Point *e* temperature (233.6ºC). In Test B, the significant reduction on Point *f* temperature, compared to Test A, demonstrates the contribution of high air pressure. The slightly higher temperature in Test D (143.5°C) than that in Test B (131.6°C) is due to the larger h_b and CP2 heat flux .

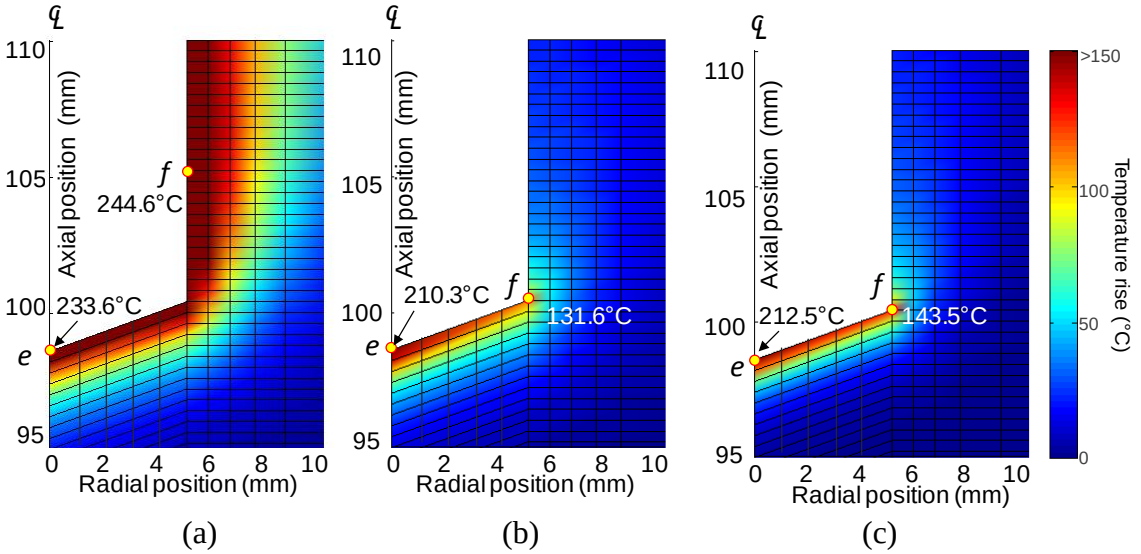

Figure 3.10 The maximum temperature on HBS (point *e*) and HWS (point *f*) around the drill tip zone at 100 mm drilling depth in (a) Test A, (b) Test B, and (c) Test C/D

3.4.4 Significance of HWS heat flux

The heat flux on HBS usually dominates the workpiece temperature in the drilling. In the deep-hole drilling, the significance of HWS heat flux in workpiece temperature could be comparable to that on HBS due to the increasing surface area and the effect of chip evacuation condition [14]. The ratio of thermal energy absorbed through HWS (denoted as H_{HWS}) to the total energy in the workpiece after drilling (denoted as H_T) was used to quantify the significance of h_w under the four drilling conditions.

H_{HWS} was estimated by integrating $h_w(x,t)$ along HWS and drilling time under the assumption that the portion of h_w in the hole region removed by the advection process and the heat dissipated from boundary were negligible. The H_T could be obtained by multiplying three terms, the workpiece mass after drilling, specific heat, and the difference of the workpiece steady state temperature after drilling and the initial temperature. The steady-state workpiece temperature was calculated by continuing the FEA after the hole drilling with adiabatic boundary condition. The thermal energy absorbed via HBS, denoted as H_{HBS}, could also be estimated by subtracting H_{HWS} from H_T. Note the H_{HBS} cannot be calculated directly from h_b since the advection process removes part of the h_b from the workpiece.

Results of H_T, H_{HWS}, and H_{HBS}, and the ratios of H_{HWS} to H_T and H_{HBS} to H_T are listed in Table 3.3. Chip accumulation in Test A resulted in high H_{HWS} (5.5 kJ) and 66% of the temperature rise in workpiece was contributed from h_w, while only 28% in Tests B and 24% in Test C. By comparing Tests B and D, doubled feed rate does not significantly affect the contribution of h_w to the workpiece temperature. For MQL deep-hole drilling without chip accumulation and clogging (Tests B, C, and D), H_{HWS} is still significant, about 1/4 of the H_T. Since most of the heat generated in the drilling is stored in chips, the high temperature chips could conduct the heat into workpiece via HWS, particularly under the MQL condition without flooding cutting fluid to cool the chips and workpiece.

Table 3.3 Contributions of thermal energy from HWS and HBS in MQL deep-hole drilling

	Test A (0-100 mm)	Test B (0-200 mm)	Test C/D (0-200 mm)
H_T (kJ)	8.36	7.89	4.58
H_{HWS} (kJ)	5.51 (66%)	2.20 (28%)	1.10 (24%)
H_{HBS} (kJ)	2.85 (34%)	5.89 (72%)	3.48 (76%)

3.5 Conclusions

This study demonstrated that the high air pressure reduced the workpiece temperature by improving the chip evacuation when the drilling feed rate was low and could not provide enough momentum to transport chips out of the hole. Modeling and experimental results also showed that no further reduction in workpiece temperature from the high air pressure if the chips could be evacuated properly under a high feed rate. Although high feed rate was benefitial to both workpiece temperature and chip evacuation, it generated higher heat flux on HBS, which could potentially cause the thermal damage on the drill.

The polynomial and bilinear CP heat flux models in the control point approach were demonstrated capable to accurately estimate the temporal and spatial change of the heat flux on HWS. The thermal energy from HWS was shown significant (about 1/4 of the total energy) in MQL deep-hole drilling even without chip accumulation and clogging problems.

The temperature showed to be a more sensitive indicator to detect the chip evacuation condition for deep-hole drilling. Chip accumulation is the transition stage between smooth chip evacuation and chip clogging, and is difficult to detect simply by measuring drilling torque. The inverse heat transfer analysis demonstrated the capability to detect the high heat flux on the HWS under chip accumulation condition.

References

[1] Stoll, A., Sebastian, A.J., Klosinski, R., Furness, R., 2008, "Minimum quantity lubrication (MQL) is a key technology for driving the paradigm shift in machining operations," SAE Paper 01-1128.

[2] Filipovic, A. and Stephenson, D., 2006, "Minimum quantity lubrication (MQL) application in automotive powertrain machining," Machining Science & Technology 10, pp. 3-22.

[3] Kamata, Y. and Obikawa, T., 2007, "High speed MQL finish-turning of Inconel 718 with different coated tools," Journal of Materials Processing Technology, 192, pp. 281-286.

[4] Rahman, M., Senthil Kumar, A., and Salam, M.U., 2002, "Experimental evaluation on the effect of minimum quantity lubricant in milling," International Journal of Advanced Manufacturing Technology, 42, pp. 539-547.

[5] Tai, B.L., Dasch, J.M., and Shih, A.J., 2011, "Evaluation and comparison of lubricant properties in minimum quantity lubrication machining," Machining Science & Technology, under review.

[6] Ke, F., Ni, J., and Stephenson, D.A., 2006, "Continuous chip formation in drilling," International Journal of Machine Tools and Manufacture, 45, pp.1652–1658.

[7] Stephenson, D.A. and Agapiou, J.S., 2006, Metal Cutting Theory and Practice, 2nd Edition, Taylor and Francis, Boca Raton, FL.

[8] Hussain, M.I., Taraman, K.S., Filipovic, A.J., and Garren, I., 2008, "Experimental study to analyse the workpiece surface temperature in deep hole drilling of aluminum alloy engine blocks using MQL technology," Journal of Achievement in Materials and Manufacturing Engineering, 31, pp. 485-490.

[9] Agapiou, J., 2010, "Development of gun-drilling MQL process and tooling for machining of compacted graphite iron (CGI)," Transactions of NAMRI/SME, 38, pp. 73-80.

[10] Bono, M. and Ni, J., 2006, "The location of the maximum temperature on the cutting edges of a drill," International Journal of Machine Tools & Manufacture, 46,

pp. 901-907.

[11] Li, R. and Shih, A.J., 2007, "Tool temperature in titanium drilling," Journal of Manufacturing Science and Engineering, 129, pp. 740-749.

[12] Fleischer, J., Pabst, J., and Keleman, S., 2007, "Heat flow simulation for dry machining of power train castings, " Annals of CIRP 56/1, pp. 17-122.

[13] Bono, M. and Ni, J., 2002, "A model for predicting the heat flow into the workpiece in dry drilling," Journal of Manufacturing Science and Engineering, 124, pp. 773-777.

[14] Tai, B.L., Stephenson, D.A., and Shih, A.J., 2011, "An inverse heat transfer method for determining workpiece temperature in MQL deep hole drilling," Journal of Manufacturing Science and Engineering, under review.

CHAPTER 4

WORKPIECE THERMAL DISTORTION IN MQL DEEP HOLE DRILLING – FINITE ELEMENT MODELING AND EXPERIMENTAL VALIDATION

ABSTRACT

This paper presents the three dimensional (3-D) finite element analysis (FEA) to predict the workpiece thermal distortion in drilling multiple deep-holes under minimum quantity lubrication (MQL) condition. Heat sources on the drilling hole bottom surface (HBS) and hole wall surface (HWS) are first determined by the inverse heat transfer method. A 3-D heat carrier consisting of shell elements to carry the HWS heat flux and solid elements to carry the HBS heat flux has been developed to conduct the heat to the workpiece during the drilling simulation. A thermal-elastic coupled FEA was applied to calculate the workpiece thermal distortion based on the temperature distribution. The concept of the heat carrier was validated by comparing the temperature calculation with an existing 2-D advection model. The 3-D thermal distortion was validated experimentally on an aluminum workpiece with four deep-holes drilled sequentially. The measured distortion on the reference point was 61 μm, which matches the FEA predicted distortion of 51 μm within uncertainty.

Contents of this chapter have been submitted as Tai, B.L., Jessop, A.J., Stephenson, D.A., and Shih, A.J., (2011), "Workpiece Thermal Distortion in MQL Deep Hole Drilling –Finite Element Modeling and Experimental Validation," *Journal of Manufacturing Science and Engineering*

4.1 Introduction

Workpiece thermal distortion is critical to the part dimensional accuracy and quality control in precision machining processes. The distortion is often caused by workpiece thermal expansion due to the conduction of heat from the tool–workpiece interface and the accumulation of high temperature chips on the workpiece surfaces [1]. The workpiece thermal distortion is significant in dry or near-dry machining at low speeds or of high aspect ratio features, such as the deep-hole drilling. There is some, but limited, research on workpiece thermal distortion in precision machining. Stephenson et al. [2] studied the thermal expansion of the workpiece in hard turning under the dry condition and reported the high heat flux flow into the workpiece. Huang and Hoshi [3] discovered that low speed face-milling could result in poor flatness due to the thermally distorted workpiece. In dry drilling, the hole geometry is often tapered with a smaller diameter at the entry due to the thermal expansion on the drill and workpiece [4-6].

The problems induced by workpiece thermal expansion are more prominent in minimum quantity lubrication (MQL) drilling of deep holes. MQL is a near-dry lubrication technique that uses a minute amount of lubricant mixed with compressed air applied directly to the cutting interface rather than flooding the workpiece with metalworking fluid. Although MQL provides equal or better lubrication, it lacks the capability to effectively cool the workpiece [7]. In addition, high-temperature chips in MQL drilling can generate a significant heat flux on the hole wall surface (HWS) in deep-hole drilling. High HWS heat flux elevates the workpiece temperature and results in poor hole quality [8]. Investigation of the hole shape has been conducted in dry and shallow hole drilling [5,6]. Tai et al. [9] has verified that, in MQL deep hole drilling, the heat flux from HWS could be comparable or greater than that of HBS. In practical MQL drilling of precision automotive powertrain components, workpiece thermal distortion has been observed to be significant enough to cause position errors in follow-up machining operations [7]. The research on hole position errors due to workpiece thermal distortion in MQL drilling of multiple holes is still lacking.

In this study, a model is developed to estimate the workpiece temperature and thermal distortion in MQL drilling of multiple deep-holes. The thermal distortion is predicted using the thermal-elastic coupled finite element analysis (FEA) based on the

workpiece temperature distribution. Several research studies have been conducted to investigate the workpiece temperature during drilling. Fleischer et al. [10] measured the steady-state workpiece temperature after drilling to estimate an average surface heat flux over time. Bono and Ni [11] developed an advection model to calculate and apply the heat flux on HBS. Kalidas et al. [12] utilized the inverse heat conduction method to determine time-independent heat fluxes from the drill point, lips, and margin to the workpiece. Tai et al. [9] applied the inverse heat transfer method to determine time-dependent heat fluxes on HWS and HBS in MQL deep-hole drilling. These workpiece thermal models of drilling [9, 11, 12] all utilize the 2-D axisymmetric FEA that involves element (or nodes) removal on HBS to mimic the drilling process. This type of FEA is suitable for modeling the drilling of a single hole in an axisymmetric workpiece. For workpieces with complex geometry and multiple holes, a 3-D model is required. The 3-D thermal-elastic coupled FEA for multi-hole drilling using the advection approach is technically challenging due to the extensive computational time required for 3-D mesh with continuous removal of the work-material and changing of workpiece geometry. In this study, a novel 3-D FEA model using heat carriers is developed to simulate the heating of the workpiece without frequent element removal during the simulation.

In this paper, the model is first introduced in Sec. 4.2. Numerical validation of the model is presented in Sec. 4.3. Experimental setups for validation of the are described in Sec. 4.4. This is followed by the presentation of thermal modeling and analysis results in Sec. 4.5. Limitations of the model and conclusions are discussed in Sec. 4.6.

4.2 Model concept

Workpiece thermal distortion is determined by the temperature change in the workpiece during the drilling of multiple holes. The model concept includes three parts: definition of heat fluxes, calculation of workpiece temperature, and thermal-elastic coupled FEA of workpiece distortion. The following three sections discuss the heat fluxes generated during deep-hole drilling on HWS and HBS, the workpiece temperature distribution calculated using the heat carrier model, and the workpiece thermal distortion due to drilling multiple holes.

4.2.1 Heat fluxes in deep hole drilling

Two heat fluxes, h_b on HBS and h_w HWS, are considered in the deep-hole drilling FEA, as shown the 2-D axisymmetric model in Fig. 4.1. The advection model [9,11] is used to calculate the workpiece temperature as the drill penetrates into the workpiece. It is achieved by removing a layer of five elements on HBS sequentially and applying h_b to the next layer. The h_w is applied on HWS along with the advection process.

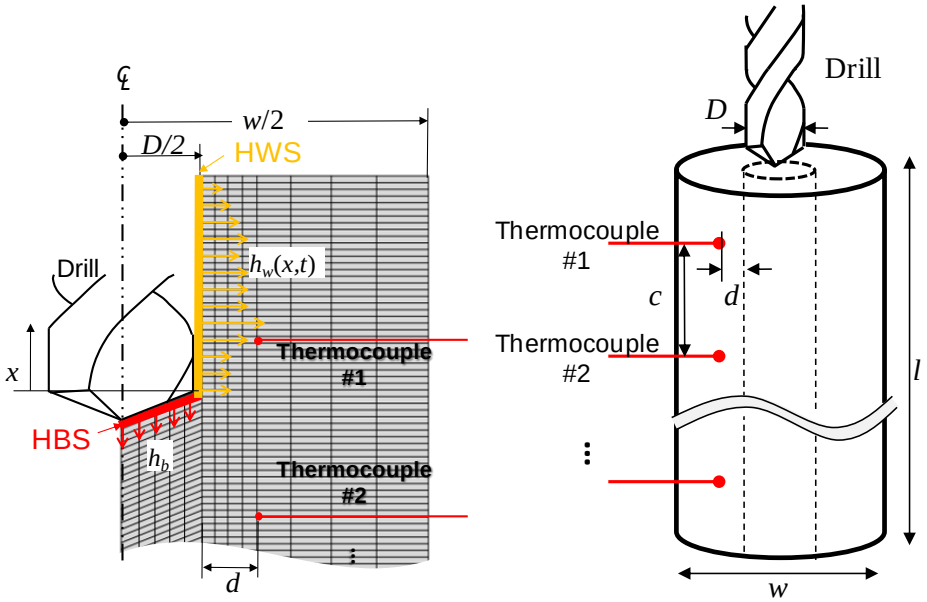

Figure 4.1 (a) 2-D axisymmetric advection FEA model and (b) the corresponding experimental setup for the inverse heat transfer method

The h_b is assumed to be time-independent and uniform on HBS based on the constant drilling feed rate and speed. The h_w varies during drilling due to the changing depth of the drill and the chip evacuation condition. As illustrated in Fig. 4.1(a), h_w is a function of time and axial position on HWS. To solve h_b and h_w under a given drilling condition, the inverse heat transfer method [9, 13] is utilized. This method is based on the temperatures measured by embedded thermocouples as the inputs. A cylindrical workpiece corresponding to the axisymmetric advection model is needed for the temperature measurement, as shown in Fig. 4.1(b), where thermocouples are located along the hole depth and close to the drilled hole surface.

4.2.2 Heat carrier model

The heat carrier model is a 3-D FEA developed in this study to simulate the workpiece temperature distribution in deep-hole drilling. As shown in Fig. 4.2(a), the heat carrier applies the constant h_b and time-dependent h_w (obtained from the inverse heat transfer method) and moves into the hole region to conduct the heat to the workpiece. The hole region is removed prior to the drilling simulation so the heat carrier can move into it. This is based on the fact that the heat transfer in the axial direction is usually much slower than the drill feed rate, thus the temperature distribution is not significantly affected by the heat carrier moving into a void space that represents the hole being drilled. This approach overcomes the practical difficulty in the 3-D advection model by eliminating the need for removing 3-D elements. As shown by the schematic of 3-D advection model in Fig. 4.2(b), the cylindrical hole region is partitioned into many advection layer regions. Unlike the 2-D advection model (Fig. 4.1(a)), which has a much simpler mesh pattern on each advection layer, the number of elements increases significantly if many thin layer regions of small 3-D elements are used. In the case of drilling multiple holes in a workpiece with complex shape, a large number of the 3-D elements are required for each hole and extensive computational time is needed. The heat carrier model illustrated in Fig. 4.2(a) simplifies the 3-D FEA procedure.

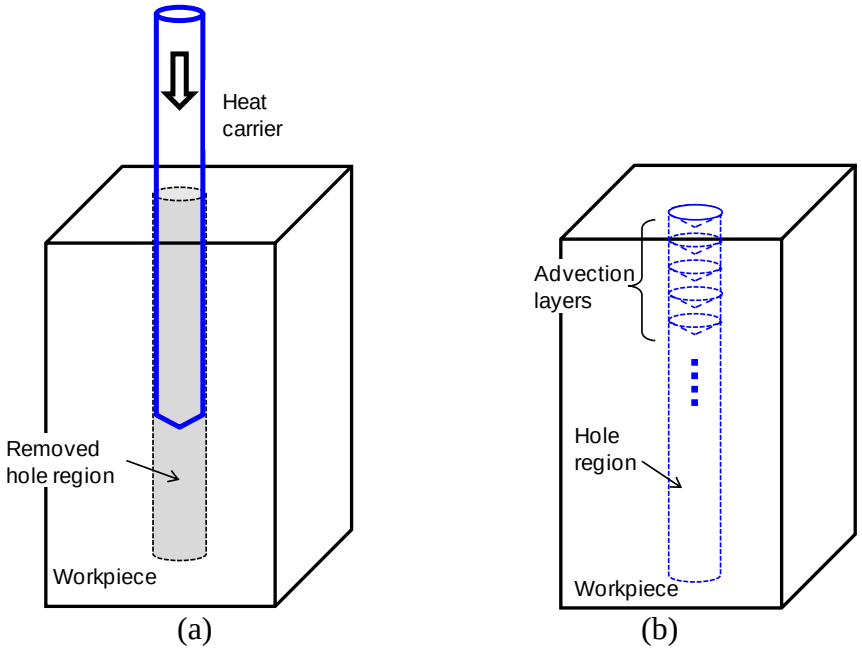

Figure 4.2 Schematics of the (a) 3-D heat carrier model and (b) 3-D advection model

As shown in Fig. 4.3(a), the heat carrier consisting of HWS and HBS carriers moves at the drilling feed rate to simulate the heat conduction to the workpiece during drilling. Since the heat carrier and workpiece have different meshes, the inconsistent mesh sizes in hole surfaces may cause the elements to intersect each other and cause the FEA to fail. Therefore, a small gap, 1% of the drill diameter, is created between matching surfaces of the hole and the heat carrier. To enable the heat transfer through the gap with nearly zero thermal contact resistance, the gap conductance is set relatively large, 10^6 W/m^2·K, in ABAQUS (version 6.8), which is the FEA software platform used in this study. Details for HWS and HBS heat carriers are described in the following sections.

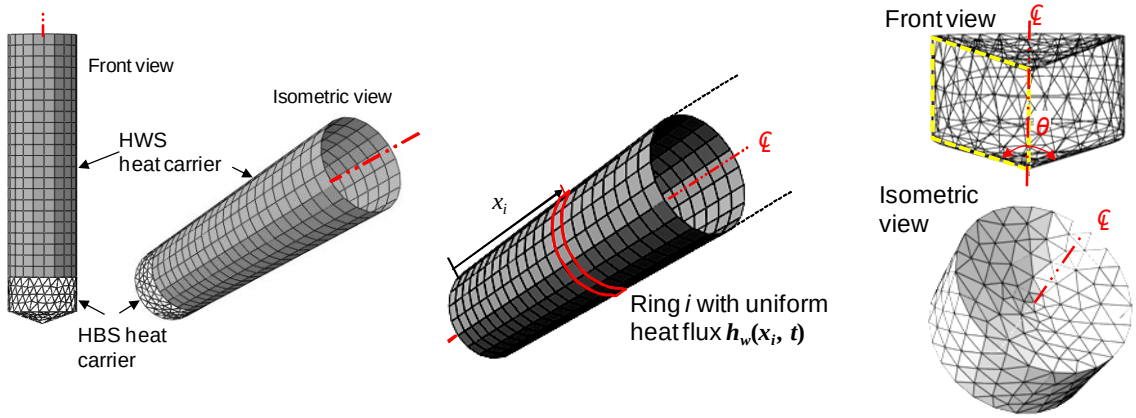

(a) (b) (c)

Figure 4.3 The 3-D heat carrier model (a) assembled heat carrier, (b) HWS heat carrier, and (c) HBS heat carrier

4.2.2.1 HWS heat carrier

The HWS heat carrier, as shown in Fig. 4.3(b), is a cylindrical shell consisting of four-node thermal-elastic coupled shell elements, S4RT in ABAQUS. The configuration of elements can be seen as many rings along the HWS carrier. The number of rings in the axial direction on the HWS heat carrier is N, which is equal to the number of time steps of h_w in the advection model for the inverse heat transfer method. The axial length of each ring in the HWS heat carrier is the distance which h_w moves within one time step in the advection model. For the ring i (= 1, 2, …, N), as highlighted in Fig. 4.3(b), the heat flux is uniformly applied with the magnitude of $h_w(x_i,t)$, where x_i is the center position of the ring i to the HBS and t is time. The heat flux at each ring varies with time as the HWS heat carrier moves into the hole.

4.2.2.2 HBS heat carrier

The HBS heat carrier, as shown in Fig. 4.3(c), is a parallelogram cross-section revolved around the centerline. The angle θ is the drill point angle. The HBS heat carrier consists of four-node tetrahedral solid element, C3D4T in ABAQUS. In the heat carrier model, since the hole region is removed before applying h_b, the heat loss caused by removing elements that store thermal energy in the advection process does not exist. A modified heat flux, denoted as h_b', on the HBS carrier provides the equivalent effect of heating the workpiece as the h_b in the advection model. The h_b' is described as h_b multiplied by a partition factor, ζ, which is between 0 and 1 and represents the ratio of heat flux that remains in the workpiece without being removed by the advection process. To determine ζ, the total amount of heat absorption during drilling, H_T, of a cylindrical workpiece is first calculated by multiplying three parameters: the steady-state workpiece temperature after hole drilling, the mass of the workpiece with drilled hole, and the specific heat of work-material. Second, using the solutions of the inverse heat transfer method, the total amount of heat flowing through HWS, H_{HWS}, can be calculated by integrating $h_w(x,t)$ by the time and spatial distribution. The partition factor for heat flowing into the workpiece through HBS is:

$$\zeta = \frac{H_T - H_{HWS}}{h_b A t_f} \tag{4.1}$$

where A is the area of HBS and t_f is the total drilling time. Thus,

$$h_b' = h_b \zeta \tag{4.2}$$

Since heat is transported to the workpiece via the side surface of the HBS heat carrier, marked as line GH of the HBS heat carrier depicted by points EFGH in Fig. 4.4, a proper axial thickness (l_b) is important. If l_b is too large, the heat carrier will store heat instead of conducting it to the workpiece. If l_b is too small, the accuracy of the temperature distribution around HBS will be affected. The l_b is determined based on an index, p (in the unit of mm), which is defined as

$$p = \frac{\alpha}{f} \tag{4.3}$$

where α is the workpiece thermal diffusivity (mm/s^2) and f is the drill axial feed rate (mm/s).

A larger p means that the heat may spread widely in the axial direction, thus an HBS heat carrier with longer l_b is needed. In general, with a constant HBS heat flux, the temperature field around the HBS would converge to a specific distribution, as illustrated in Fig. 4.4, when drilling is beyond a certain depth. This phenomenon can be observed during the advection modeling. The l_b is determined by the ratio, k, which is defined by

$$k = \frac{T_E - T_F}{T_E - T_0} \tag{4.4}$$

where T_E and T_F are the temperatures at Points E and F (Fig. 4.4) respectively, and T_0 is the initial temperature of the workpiece. The optimal value of k is determined by matching the results of the 2-D axisymmetric advection model and the HBS heat carrier model, as in the example presented in Sec. 4.3.1.

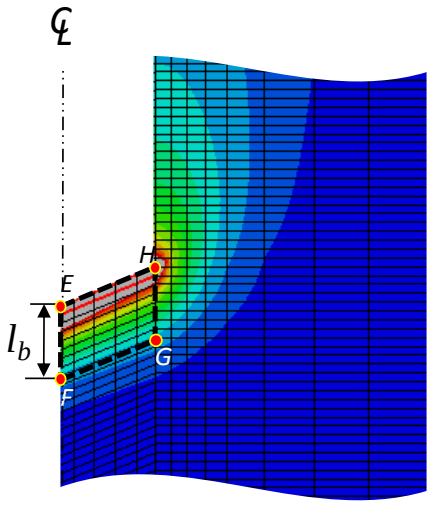

Figure 4.4 Definition of axial thickness (l_b), the geometry (EFGH) of the 2-D axisymmetric HBS heat carrier, and convergent temperature distribution due to constant HBS heat flux

4.2.3 Workpiece thermal distortion in multi-hole drilling

The workpiece thermal distortion in drilling multiple deep holes is predicted based on the workpiece temperature using FEA. The heat carrier model is applied sequentially for each hole drilling to predict the workpiece temperature distribution. The temperature distribution of the workpiece in the previous hole drilling is used as the initial condition for the next hole. Thus, the temperature is accumulated and transported in the workpiece as holes are drilled sequentially. The holes in the workpiece are removed sequentially throughout drilling analysis. For example, the region for the first hole is removed at the beginning of analysis and the heat carrier is inserted into the hole to conduct the heat. After the heat carrier reaches the end of the hole, the heat transfer in the workpiece continues the period of time it takes the spindle to retract and move to the second hole position. At the start of the second hole drilling, the region for the second hole is removed and the heat carrier is inserted with the same heat fluxes. This procedure is repeated in follow-up holes.

To predict the thermal distortion, a separate thermal-elastic FEA is applied to avoid solving the displacement and temperature simultaneously, which requires extensive computation time in 3-D FEA. Furthermore, the expansion of the workpiece and heat carrier would create contact between the two and cause computational errors. This approach calculates the temperature distribution first. For the specific time step of interest, the temperature field is extracted and imported into the thermal-elastic FEA to calculate the workpiece thermal distortion.

4.3 Numerical Validation

The heat carrier model was validated numerically by comparing the calculated workpiece temperature with the existing solution using the 2-D advection model [13]. The selected case was drilling a 10 mm diameter, 200 mm deep hole along the centerline of a 40 mm diameter solid, cylindrical, ductile iron workpiece. By applying the heat fluxes h_b (= 3.10 MW/m^2) and $h_w(x,t)$ in the advection model [13], the steady-state workpiece temperature can be obtained. Consequently, the H_T = 7.89 kJ and H_{HWS} = 2.20

kJ is calculated. Using Eq. (4.1) with t_f = 50 s, ζ = 48% is calculated, and therefore h_b' = 1.49 MW/m^2.

The validation includes two parts: one verifies the HBS heat carrier model and l_b (Sec. 4.3.1) and the other compares the difference of workpiece temperature predicted using the 2-D advection and 3-D heat carrier models (Sec. 4.3.2).

4.3.1 HBS heat carrier model validation

To find the optimal k for the axial thickness (l_b) and validate the modified heat flux (h_b'), a 2-D axisymmetric HBS heat carrier, converted from the 3-D HBS heat carrier (Fig. 4.3(c)) with only h_b' applied, was compared with the 2-D advection model with only h_b applied. The model had 140° point angle and 10 mm diameter hole (the drill used in this study). Based on the work-material and drilling feed rate, p can be determined to calculate l_b with a given k value, as described in Sec 4.2.2.2. The optimal k is selected from four values, 80%, 70%, 60%, and 50%, with an interval of 10% since k does not significantly affect the overall workpiece temperature. In the case of a ductile iron workpiece and 4 mm/s feed rate, α is 6.89 mm^2/s and p is 1.72 mm. Figures 4.5(a) and (b) show the temperature distributions at 100 mm drilling depth in the 2-D advection mode and the heat carrier model with k = 60% (l_b=1.6 mm), respectively. Temperature distributions of a 16 mm by 8 mm region highlighted in Figs. 4.5(a) and (b) were overlaid in Fig. 4.5(c) for comparison. The best R^2 (= 0.97) was found for k = 60%. By testing k values under different p (adjusted by feed or material properties), the optimal k was also found either 50% or 60%. In this study, k = 60% was selected to find l_b.

To cover a wide range of feed rates on different work-materials, as shown in Fig. 4.6, six cases ranging from p = 0.4 mm to 13.7 mm were applied in the advection model to find the corresponding l_b based on the temperature distribution and k = 60%. This range includes the drilling conditions for iron at 0.5 mm/s to 16 mm/s feed rate and aluminum at 5.5 mm/s to 150 mm/s feed rate. Therefore, the l_b can be obtained from Fig. 4.6 with a given work-material and drilling feed rate for a specific type of drill.

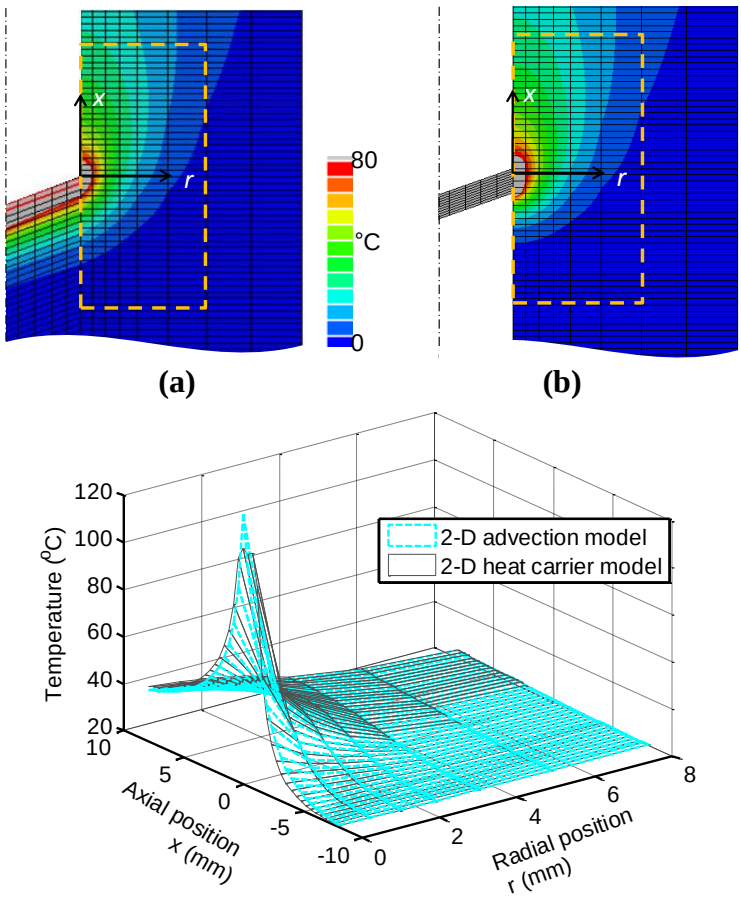

Figure 4.5 Temperature distributions around HBS in (a) 2-D advection model and (b) 2-D HBS heat carrier with k = 60%, and (c) the comparison of temperature results in the regions highlighted in (a) and (b)

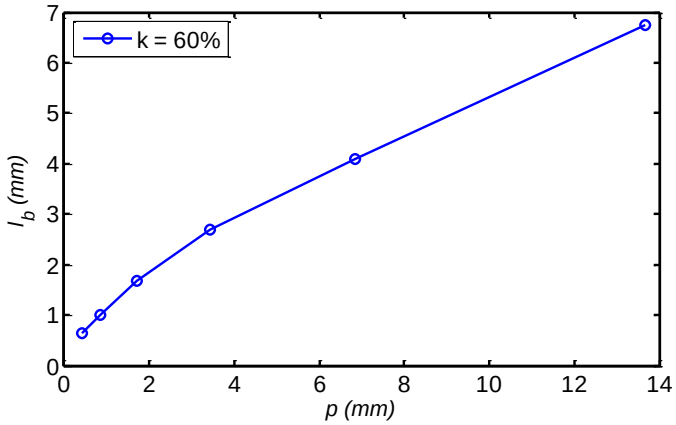

Figure 4.6 The l_b determined by index p ranging from 0.4 to 13.7 mm with k = 60%

4.3.2 3-D heat carrier model validation

The assembled heat carrier (Fig. 4.3(a)) was applied in 3-D FEA with a cylindrical workpiece model to calculate the temperatures at selected positions for comparison with the 2-D advection modeling results. For the 3-D HBS heat carrier, the size and shape correspond to the 2-D axisymmetric HBS heat carrier in the previous section with l_b = 1.6 mm. For the HWS heat carrier, there were 125 rings on the 200 mm long cylindrical shell. The model's initial temperature was set to 20°C. Figure 4.7(a) shows the workpiece surface temperature at time 24.8 s (= 99.2 mm drilling depth) using the 3-D heat carrier model. The highest surface temperature is about 30°C at 50 mm from the top surface. As shown in Fig. 4.7(b), five points that are 3.4 mm from HWS and positioned along the axial length were selected to compare the temperature vs. time predicted using both models. The maximum discrepancy, as shown in Fig. 4.7(b), is about 5% at the peak temperature. At the end of drilling, the average temperatures at the five points are 31.3˚C and 31.9°C for the 3-D heat carrier and 2-D advection models, respectively. Overall, the agreement of the results from each model validates the proposed 3-D heat carrier model.

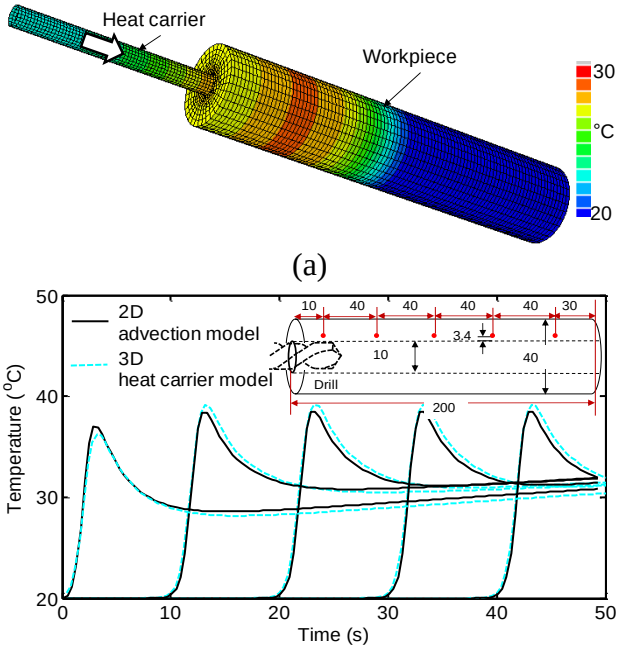

Figure 4.7 (a) Surface temperature at 24.8 s drilling time in 3-D heat carrier model and (b) temperature comparison between 3-D heat carrier model and 2-D advection model

4.4 Experimental Setups

The deep hole drilling experiment was conducted on a Fadal vertical machining center (Model VMC 4020). The feed rate and spindle speed were set at 0.2 mm/rev and 2100 rpm, respectively. A 10 mm diameter, 220 mm long solid carbide drill with oil feed holes (Titex, Model A6785TFP-10) was used. An AMCOL fluid delivery system was used to supply the MQL fluid and air mixture. The compressed air supply for the MQL system was regulated to 500 kPa (5 bar). The MQL fluid was Milacron CIMFREE VG-703ES. The flow rate was approximately 60 mL/h while at 2100 rpm spindle speed.

Aluminum 6061-T6 was chosen as the work-material in this study. Two sets of experiments were conducted in this study. The first, Setup I, was the drilling of a cylindrical workpiece for the inverse heat transfer solutions of heat fluxes (h_b and h_w). The second, Setup II, was to validate the thermal distortion predicted by the 3-D heat carrier model.

4.4.1 Setup I – Determination of drilling heat fluxes

Figure 4.8 shows Setup I, used to find the HBS and HWS heat fluxes. The cylindrical workpiece was 38 mm in diameter and 152 mm in length. Five Type E thermocouples (OMEGA Model 5TC-TT-E-36-72) with 0.127 mm wire diameter were embedded in the workpiece at 3.4 mm from HWS and 30 mm apart from each other. These thermocouples are marked as TC1, TC2, TC3, TC4, and TC5 in Fig. 4.8. The 3.4 mm distance to HWS was chosen to avoid the large temperature gradient near HWS, which could potentially cause measurement errors and affect the accuracy of the heat flux estimation [9]. The thermocouple holes were 1.2 mm in diameter and filled with the thermal paste to minimize the thermal contact resistance. A 10 mm diameter through hole was drilled at the center of the workpiece under the MQL condition using the 10 mm diameter carbide drill. The total drilling time was 21.7 s. The temperatures were recorded at a 10 Hz sampling rate.

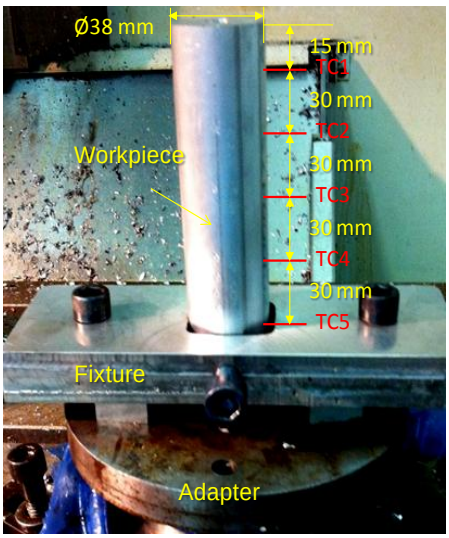

Figure 4.8 Setup I: Cylindrical workpiece with five thermocouples embedded along the depth for the inverse heat transfer method

4.4.2 Setup II – Workpiece thermal distortion

Figure 4.9(a) shows the shape and dimensions of the workpiece in Setup II, used to measure the workpiece thermal expansion after the MQL drilling of four deep holes. A picture of the experimental setup for Setup II is shown in Fig. 4.9(b). The workpiece was a 50.8 mm × 152 mm × 152 mm aluminum block with a 25.4 mm deep and 25.4 mm wide region sticking out of the bottom on one side for clamping. This design avoided introducing significant constraints to the workpiece thermal expansion in the X-direction (marked in Fig. 4.10(a)) during drilling. The origin of the XYZ coordinate system was set at the corner of the top surface (Point O in Fig. 4.9(a)).

Four 152 mm deep through holes, marked as #1, #2, #3, and #4 in Fig. 4.10(a), were drilled into the workpiece in sequence using the same drill, spindle speed, and feed rate as in Setup I. Four reference holes, marked as *a*, *b*, *c*, and *d*, were drilled 18 mm deep with a 9.5 mm drill. Holes *a* and *b* were drilled prior to drilling the four deep holes. Holes *c* and *d* were drilled right after the drilling of four deep holes. The difference of distance in the X-direction between holes *a* and *b* to holes *c* and *d* and the programmed nominal X-position (127.0 mm in Fig. 4.9(a)) in the machine determines the experimentally measured thermal expansion of the workpiece.. This experimental measurement is compared with the predicted thermal expansion in the X-direction using 3-D heat carrier model.

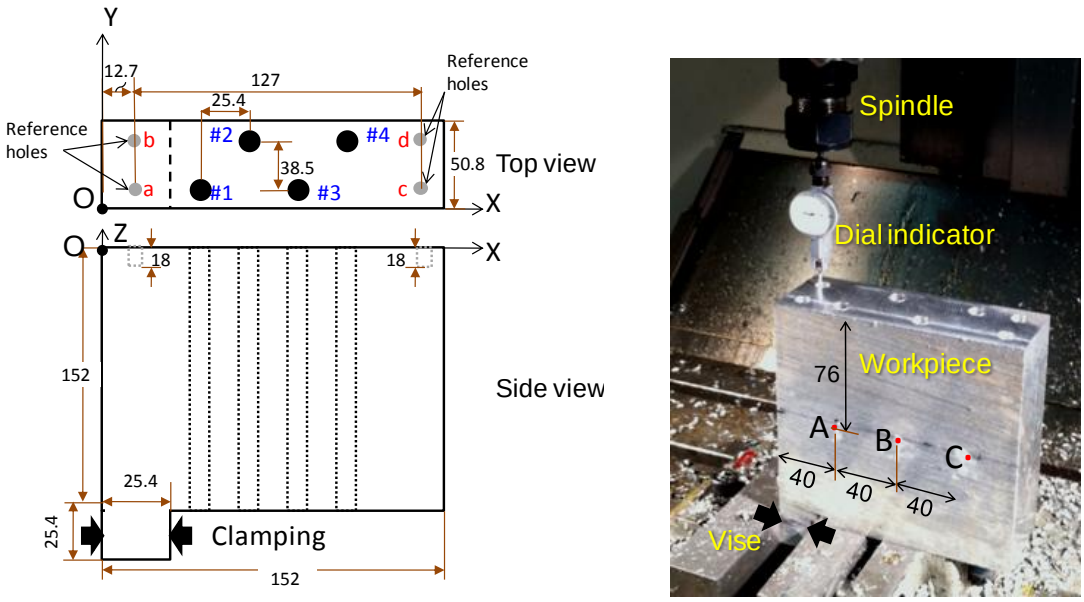

(a) (b)

Figure 4.9 Setup II: (a) workpeice design for thermal distortion experiment and (b) the measurement of hole positions using dial indicator (unit: mm)

The position of reference holes were measured by using a dial indicator on the machine spindle, as shown in Fig. 4.9(b), after the workpiece was cooled to the room temperature. The accuracy of the machine's positioning in the X axis was measured with a Renishaw laser interferometer (Model ML 10). The machine axis resolution was 2 µm. Laser interferometry measurements showed the machine X axis position error was below 5 µm. The resolution of the dial indicator was also below 5 µm. The hole position measurement error using the dial indicator in the machine was estimated to be less than 10 µm.

For validating the workpiece temperature in FEA, three thermocouples, marked as A, B, and C, as shown in Fig. 4.9(b), were attached on the workpiece surface and recorded the surface temperature during drilling.

4.5 Modeling and experimental results

The inverse heat transfer solution of h_b and h_w, workpiece temperature, and workpiece thermal distortion are presented in the following three sections.

4.5.1 Heat fluxes on HBS and HWS (Setup I)

Using the measured temperatures at five thermocouples (Fig. 4.10(a)), the heat fluxes were determined based on the inverse heat transfer method [9]. The calculated h_b is 4.5 MW/m^2. The h_w, as a function of time and drill position, is shown in Fig. 4.10(b). By applying the heat fluxes in the 2-D advection model, the calculated temperatures at the five thermocouple positions were compared with the measured data in Fig. 4.10(a). The overall good agreement between the FEA and measured temperatures verify the inverse heat transfer method for aluminum work-material, which had not been tested in our previous study [9, 13]. There is some discrepancy for TC1 in the early stage of drilling (2 to 5 s). This phenomenon has been observed [13] due to the fast heat flux change that cannot be captured by the h_w model in the inverse heat transfer method. Two tests were conducted under the same drilling condition in this experiment and generated repeatable temperature data.

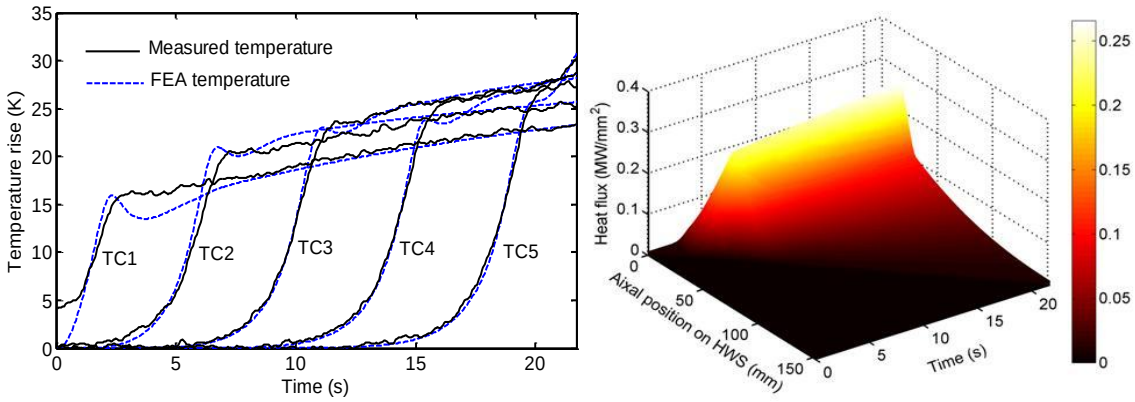

(a) (b)

Figure 4.10 Results of the inverse heat transfer method: (a) measured and FEA calculated temperatures at thermocouple positions and (b) temperoal and spatial distribution of h_w

4.5.2 Workpiece temperature (Setup II)

The 3-D heat carrier model was established based on the experimental condition. For the HBS heat carrier, the diffusivity of aluminum 6061 was 74.4 mm^2/s and the drilling feed rate was 7 mm/s, thus the index p was 10.6 mm. Based on Fig. 4.5 with k = 60%, the HBS carrier thickness l_b was determined to be 5.6 mm. For the HWS heat carrier, 100 rings of elements (N=100) were created along the 152 mm length. This

corresponded to 1.52 mm ring axial length, which was finer than that in the validation case (1.6 mm) in Sec 3. The time-dependent h_w (Fig. 4.10(b)) calculated by the inverse heat transfer method was applied on each ring.

The 3-D FEA mesh of the workpiece prior to inserting the heat carrier to hole #1 is shown in Fig. 4.11. The elements were 8-node thermally coupled bricks (C3D8T). The region for hole #1 had been removed. The heat carrier (Fig. 4.3(a)) moved at a speed of 7 mm/s (feed rate of the drill) into the hole to conduct heat fluxes (h_w and h_b') into the workpiece. Figure 4.12(a) shows the surface temperature distribution at the time when the heat carrier penetrates the bottom of the workpiece for hole #1. The highest temperature is close to the bottom of the workpiece, near hole #1. The temperature distribution in the workpiece after 6.5 s taken to retract the drill and move to the position for hole #2 is shown in Fig. 4.12(b), which is also the initial temperature field in hole #2 analysis. The region for hole #2 was then removed, the workpiece was remeshed, and the heat carrier was inserted to deliver heat fluxes. The workpiece temperature after drilling hole #2 is shown in shown in Fig. 4.12(c). Similarly, the temperature distributions after drilling holes #3 and #4 are shown in Figs. 4.12(d) and (e), respectively. The higher temperature region visible in Fig. 4.12(d) is due to hole #3 being close to the workpiece front surface. The gradual increase of overall workpiece temperature can be observed as the holes are drilled sequentially.

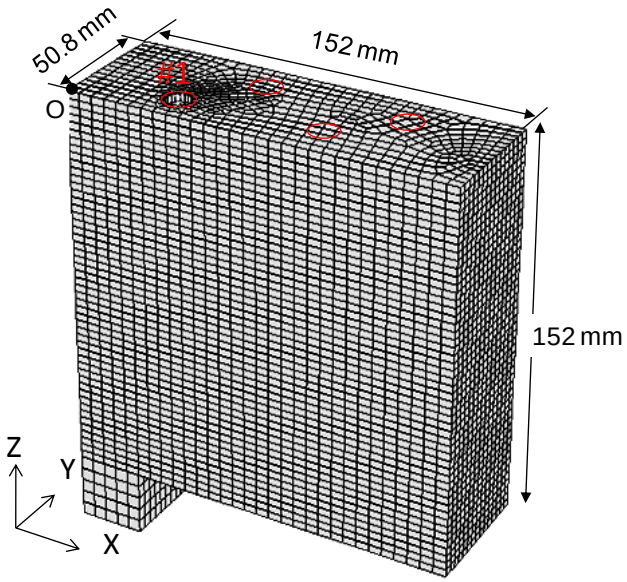

Figure 4.11 The 3-D FEA mesh of the workpiece for multi-hole drilling

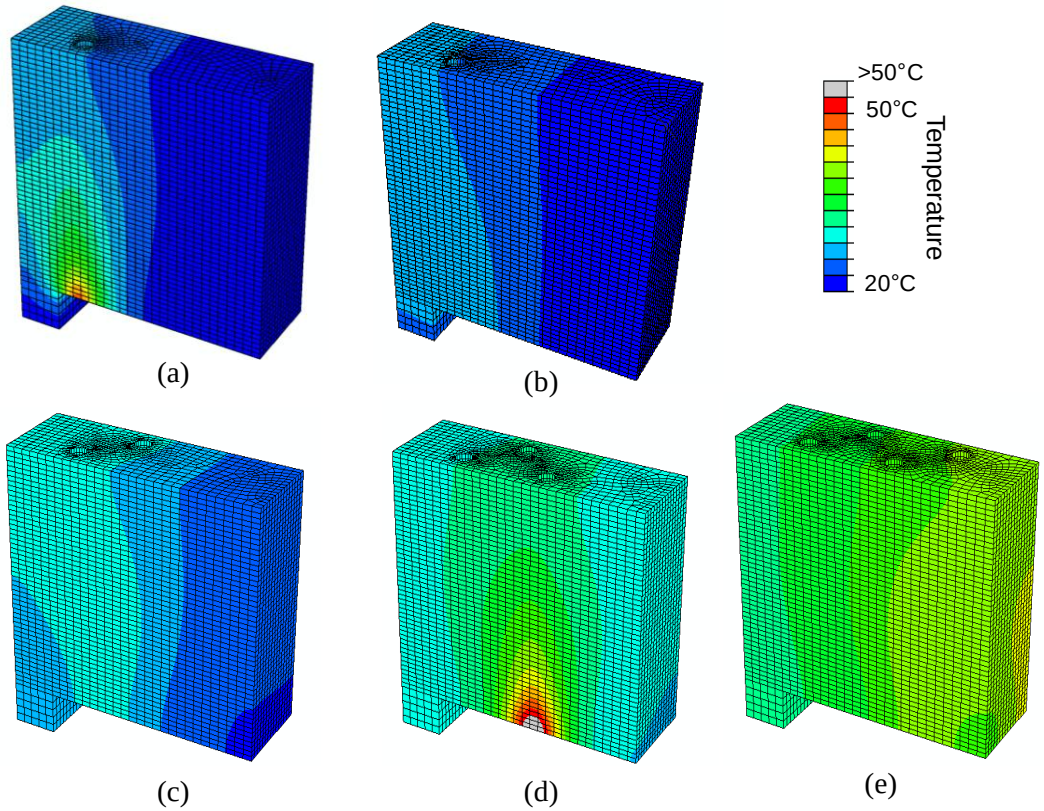

Figure 4.12 Workpiece Temperature distribution at (a) the end of drilling hole #1, (b) 6.5 s after the end of drilling hole #1, and the end of drilling (c) hole #2 (d) hole #3 (e) hole#4

Temperatures at Points A, B, and C (Fig. 4.9) were extracted from FEA and compared to experimental measurements. As shown in Fig. 4.13, these temperatures match very well except near the peak at Points A and B. Further investigation shows that the discrepancy is due to the limitation of h_w spatial resolution close to the drill tip.

There was a 22 s time lag for tool change and positioning the drill for the reference holes *c* and *d*. The workpiece temperature distributions in the front and back of the workpiece are shown in Fig. 4.14. This is the temperature distribution used for the thermal-elastic FEA to calculate the workpiece thermal distortion. The peak temperature is about 37.5°C at the corner of the workpiece bottom close to hole #4. The low temperature is 31.5°C is close to hole #1. The temperature gradient is observed along the X-direction.

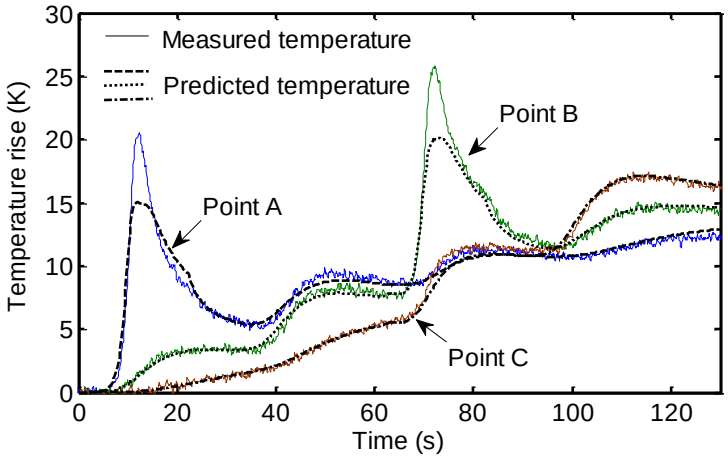

Figure 4.13 Measured and predicted surface temperatures at Points A, B, and C

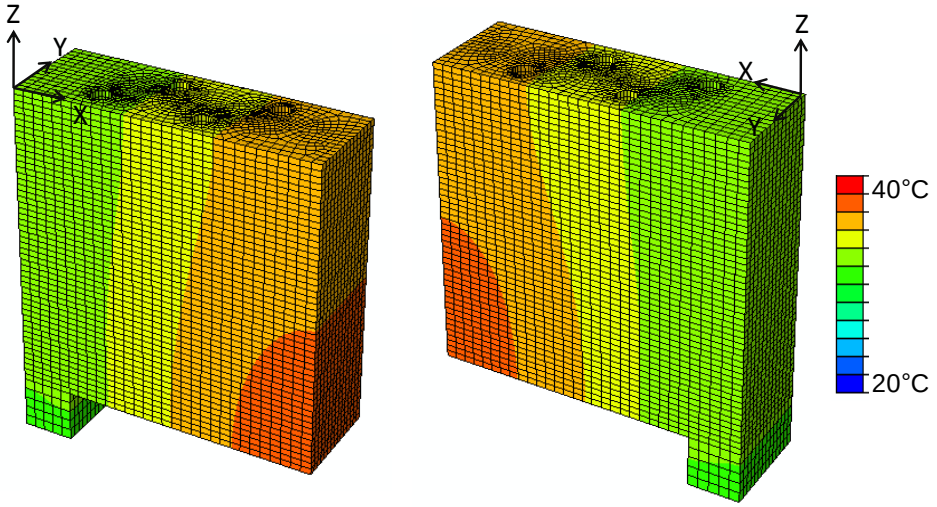

Figure 4.14 Two viewpoints of workpiece temperature distribution in 22 s after the end of hole #4 drilling

4.5.3 Workpiece distortion (Setup II)

The temperature distribution in Fig. 4.14 was re-meshed to the 8-node linear brick element (C3D8R in ABAQUS) and the thermal-elastic FEA was performed to simulate the workpiece thermal expansion. The FEA predicted workpiece thermal expansion in the X-direction is shown in Fig. 4.15, where the contour represents the displacement in X-direction. The workpiece thermal distortion across the YZ plane is almost uniform.

The FEA model predicted that the thermal expansion between two sets of reference holes (holes *c* and *d* vs. holes *a* and *b*) is 51 μm. This is comparable to the

experimentally measured 61 µm. With the potential measurement error of 10 µm, the proposed FEA 3-D heat carrier and thermal distortion model for predicting the workpiece thermal distortion in MQL deep-hole drilling is valid.

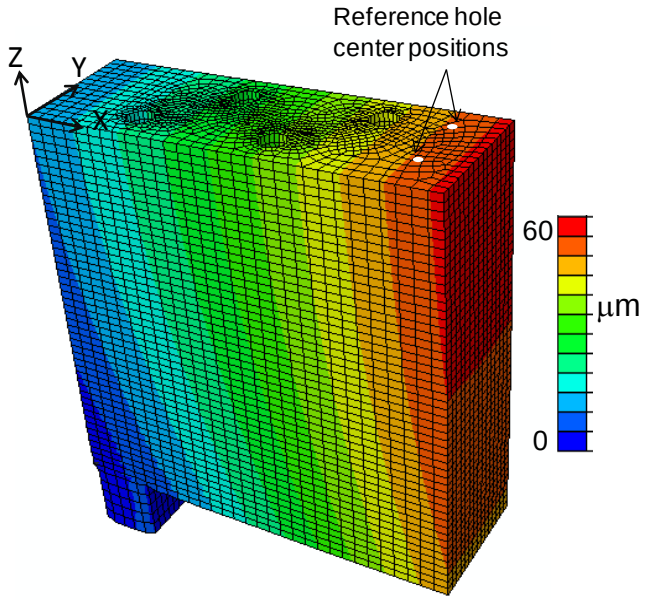

Figure 4.15 Simulated workpiece distortion in X-direction at the start of drilling the reference holes

4.6 Conclusions

In this study, the heat carrier model was proposed and verified to predict the 3-D workpiece temperature distribution and thermal distortion. This approach has demonstrated to be practical, universal, computationally time efficient, and feasible to study the thermal distortion of MQL multi-hole drilling. The method could be used to design the clamping layout to minimize thermal distortion, for selection of machining parameters, as well as for error compensation in the MQL machining operations to improve machining accuracy. Heat fluxes of this thermal distortion model were assumed to be repeatable at each hole drilling. The effect of drill wear and gradual increase in drilling force, torque and heat fluxes could be included in future study.

In the heat carrier model, the method of removing the entire hole prior to the drilling would remove some of the heat that potentially conducts through the workpiece during the time of drilling a previous hole. The error associated with this method is

limited if the distance between holes is large or the drill feed rate is relatively fast compared to the thermal diffusion of the work-material. To minimize this potential error, a deep hole can be divided into several segments and then removed sequentially. This step-removal approach is investigated in this study by dividing each hole into three equally long segments. In total, twelve segments for the four holes were removed and the heat carrier inserted into each of the segments sequentially. For example, Fig. 4.16(a) shows the removed 1st segment of hole #2 with the heat carrier mid-way through this segment. Figs. 4.16(b) and (c) show the removal of 2nd and 3rd segments of hole #2, respectively, with the heat carrier inserted further. The discrepancy between the initial approach and the step-removal approach of temperatures at Points A, B, and C 22 s after drilling hole #4 was only 0.3%. This confirmed that the step-removal approach is not necessary in this study.

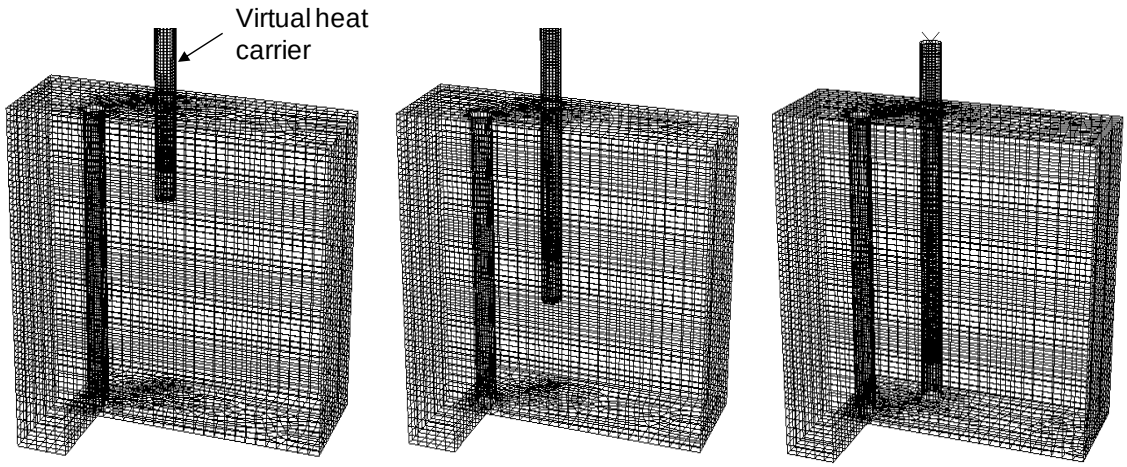

(a) (b) (c)

Figure 4.16 Step-removal approach in the heat carrier model

References

[1] Stephenson, D.A, and Agapiou, J.S., Metal Cutting Theory and Practice, 2nd Edition, Taylor and Francis, Boca Raton, FL, 2006.

[2] Stephenson, D.A., Barone, M.R., and Darqush, G.F., 1995, "Thermal Expansion of the Workpiece in Turning," Journal of engineering for industry, 117, pp. 542-550

[3] Huang, Y., and Hoshi, T., 2000, Improvement of Flatness Error in Milling Plate-shape Workpiece by Application of Side-clamping Force, Precision Engineering, 24, pp. 364-370.

[4] Haan, D. M. , Batzer, S.A., Olson, W.W., and Sutherland, J.W., 1997, "An experimental study of cutting fluid effects in drilling," Journal of Materials Processing Technology, 71, pp. 305-313

[5] Bono, M., and Ni, J., 2001, "The Effects of Thermal Distortions on the Diameter and Cylindricity of Dry Drilled Holes," International Journal of Machine Tools and Manufacture, 41, pp.2261-2270.

[6] Kalidas, S., Kapoor, S.G., and DeVor, R.E., 2002, "Influence of Thermal Effects on Hole Quality in Dry Drilling, Part 2: Thermo-Elastic Effects on Hole Quality," 124, pp.267-274

[7] Stoll, A., Sebastian, A.J., Klosinski, R., and Furness, R., 2008, "Minimum Quantity Lubrication (MQL) is a Key Technology for Driving the Paradigm Shift in Machining Operations," SAE Paper 01-1128

[8] Agapiou, J., 2010, "Development of Gun-Drilling MQL Process and Tooling for Machining of Compacted Graphite Iron (CGI)," Transactions of NAMRI/SME, 38, pp.73-80

[9] Tai, B.L., Stephenson, D.A., and Shih, A.J., 2011, "An Inverse Heat Transfer Method for Determining Workpiece Temperature in MQL Deep Hole Drilling," Journal of Manufacturing Science and Engineering, submitted.

[10] Fleischer, J., Pabst, J., and Keleman, S., 2007, "Heat Flow Simulation for Dry Machining of Power Train Castings," Annals of CIRP 56/1, pp. 117-122

[11] Bono, M., and Ni, J., 2002, “A Model for Predicting the Heat Flow into the Workpiece in Dry Drilling,” Journal of Manufacturing Science and Engineering 124, pp.773-777.

[12] Kalidas, S., Kapoor, S.G., and DeVor, R.E., 2002, “Influence of Thermal Effects on Hole Quality in Dry Drilling, Part 1: A Thermal Model of Workpiece Temperatures,” 124, pp.258-266

[13] Tai, B.L., Stephenson, D.A., White, S.B., and Shih, A.J., 2011, “Investigation of Air Pressure and Feed Rate Effects on Workpiece Temperature in MQL Deep Hole Drilling Using the Inverse Heat Transfer Method,” International Journal of Machine Tools and Manufacture, submitted.

CHAPTER 5
CONCLUSIONS AND FUTURE WORK

5.1 Conclusions and major contributions

This dissertation studied the workpiece temperature and the associated thermal distortion in MQL deep-hole drilling. A quantitative and fundamental understanding of the heat flow into workpiece in MQL deep-hole drilling was developed. The proposed methodologies have demonstrated to be feasible to determine the heat fluxes during drilling and to visualize workpiece temporal and spatial temperature distributions and the associated thermal distortion.

Major achievements of this dissertation can be summarized in two parts:

(1) *Deep-hole drilling HWS heat flux*: The HWS heat flux as a function of time and depth to include the effects of complicated interactions on HWS was determined using the inverse heat transfer method developed in this study. Two approaches were introduced in this method. The first approach divided the hole into segments, each with a thermocouple. This approach was able to estimate the dramatic heat flux change due to unstable chip evacuation, such as in dry deep-hole drilling, with many temperature inputs along the depth. The other was the control-point approach which required less, 3 to 5, thermocouples, independent of the hole depth, to find the HWS heat flux under a stable drilling condition (no chip clogging). The control point approach was more suitable for deep-hole drilling evaluation, while the first approach could be used to study the chip clogging effects. The constant HBS heat flux calculated by this inverse method was also verified to be consistent with the theoretical drilling model using torque, thrust force, and drill geometry as inputs.

(2) *Workpiece thermal distortion in drilling multiple deep-holes:* The heat carrier model was developed and validated to accurately predict the temperature distributions and thermal distortions of a 3-D workpiece with multiple holes drilled sequentially. The model was able to analyze the drilling heat transfer within in an efficient computational time since no mechanical contact and elements removal were involved. This method could be used to design the clamping layout to minimize the thermal distortion, for selection of the machining parameters, and also for error compensation in the MQL machining operations to improve the machining accuracy. The effect of drill wear and gradual increase in drilling force and torque and heat fluxes could be included in future study.

The conclusions and important findings in this research can be summarized as follows:

(1) The contribution of HWS heat flux to the workpiece temperature was significant in deep hole drilling due to the increasing surface area with drilling depth and the change of chip evacuation condition.

(2) Early detection of chip accumulation using drilling torque and force measurement might not be feasible. The workpiece temperature could be a more sensitive indicator for detection of chip accumulation problem in deep hole drilling.

(3) High air pressure in MQL deep-hole drilling improved the chip evacuation and consequently reduced the chips-induced heat flux on HWS. However, it did not provide further improvement if the chips are evacuated properly under certain depth, feed, and speed.

(4) Higher feed rate (high feed and spindle speed) led to lower workpiece temperature, but also generated higher heat fluxes on the HWS and HBS, which could potentially cause hole distortion and thermal damage on the drill.

(5) The 3-D heat carrier model demonstrated that significant thermal distortion could occur in drilling aluminum-based work-materials.

5.2 Future work

The methodologies and models proposed in this research could be further improved and /or extended in the following directions:

(1) Drilling is also a common operation in surgery. This research can be applied to study the potential thermal damage in the neurosurgery. The deep-hole drilling is used to reach the tumor inside the brain through the skull. Due to high drill rotational speed and lack of irrigation during drilling, the temperature in the bone and nerve tissue surrounding the hole can rapidly increase and the heat can spread out to create damage to the nerves. The drill and operating parameters are usually designed and selected based on the surgeon's feeling. The inverse heat transfer method can be further advanced to understand the bone temperature in drilling during the surgery. The better drill design, machining parameters, and irrigation method can be developed.

(2) The proposed inverse heat transfer method and thermal model will be applied to investigate the workpiece temperature and thermal distortion in deep hole drilling on automotive engine block, engine head, and crankshaft.

(3) The error compensation strategies, workpiece clamping forces and locations, and machining parameters can be developed based on minimizing the thermally-induced errors in deep hole drilling.

(4) For the inverse heat transfer method, a time-dependent HBS heat flux can be explored. The time-independent heat flux in this research is based on the constant drilling feed and speed. In fact, the continuous cutting process can raise the drill tip temperature to conduct more heat to the workpiece.

(5) The temperature-dependent mechanical and thermal properties can be included in the thermal distortion analysis. In the low-conductivity material, the temperature around the hole region can be high enough to cause material softening.

(6) The hole cylindricity and straightness due to thermal distortion can be calculated theoretically using the heat carrier model and validated with experimental measurements of hole geometry.